

Basin modelling of a complex rift system: The Northern Vøring Volcanic Margin case example

Sébastien Gac¹  | Mansour M. Abdelmalak^{1,2}  | Jan Inge Faleide^{1,2,3}  |
Daniel W. Schmid^{3,4,5}  | Dmitry Zastrozhnov^{6,7,8} 

¹Centre for Earth Evolution and Dynamics (CEED), Department of Geosciences, University of Oslo, Oslo, Norway

²Research Centre for Arctic Petroleum Exploration (ARCEX), University of Tromsø, Tromsø, Norway

³Department of Geosciences, University of Oslo, Oslo, Norway

⁴Physics of Geological Processes (PGP), Department of Geosciences, University of Oslo, Oslo, Norway

⁵GeoModelling Solutions GmbH, Zurich, Switzerland

⁶Volcanic Basin Petroleum Research AS, Oslo, Norway

⁷A.P. Karpinsky Russian Geological Research Institute (VSEGEI), Saint-Petersburg, Russian Federation

⁸Institute of Earth Sciences, Saint-Petersburg State University, Saint-Petersburg, Russian Federation

Correspondence

Sébastien Gac, Centre for Earth Evolution and Dynamics (CEED), Department of Geosciences, University of Oslo, Oslo 0316, Norway.
Email: sebastien.gac@geo.uio.no

Funding information

Norges Forskningsråd, Grant/Award Number: 223272; Lundin Norway; Aker BP; Vær Energi

Abstract

Extensional processes can lead to complex crustal configuration depending on the mechanisms of lithospheric thinning and the impact of magmatic additions during rifting and breakup. In this context, we studied the Vøring volcanic passive margin offshore Norway. The evolution of the inner Vøring Margin is well explained by standard models of lithosphere extension. However, these models fail to reproduce key observations at the outer (volcanic) province such as regional uplift at the time of breakup and excess magmatism. Therefore, additional processes are required to explain these observations. Excess magmatism and uplift have been related to mantle processes such as the arrival of the hot Icelandic mantle 'plume' or small-scale convection processes. Melt retention in the asthenosphere has also been proposed to explain uplift. At last, mantle phase transitions during extension may contribute to uplift. We present tectonic and thermal models of basin evolution along a seismic profile crossing the Northern Vøring Margin. The thermal and isostatic history of basins is constrained through time-forward basin modelling based on an automated inverse basin reconstruction approach. Two scenarios are evaluated: The first one includes pronounced mantle stretching during the last late Cretaceous-Paleocene rifting event, and the second one includes late Paleocene-early Eocene mantle thinning, at the breakup time around 56–54 Ma. Models incorporating late Paleocene-early Eocene mantle thinning and taking into account magmatic processes (melt retention and magmatic underplate) and mantle phase transitions satisfactorily reproduce the specific observations of the outer (volcanic) margin. This result supports the contribution of the hot Iceland plume on the evolution of the Vøring Margin. Our results also indicate that thin-crust models can produce a partially serpentinized mantle beneath the highly extended parts of the Vøring Basin. However, this model fails to reproduce observations. This suggests that serpentinization can occur locally but could not explain the entire lower crustal body nature.

This is an open access article under the terms of the Creative Commons Attribution License, which permits use, distribution and reproduction in any medium, provided the original work is properly cited.

© 2021 The Authors. *Basin Research* published by International Association of Sedimentologists and European Association of Geoscientists and Engineers and John Wiley & Sons Ltd.

KEYWORDS

basin modelling, magma processes, mantle phase transitions, serpentinization, uplift, volcanic margin

1 | INTRODUCTION

Lithosphere extension models (McKenzie, 1978) are usually proposed to explain the formation of extensional sedimentary basins and continental passive margins. The key parameter of these models is the crustal stretching factor β that characterizes the magnitude of crustal extension. Information on stretching factors is preserved in the presently observed stratigraphy. Basin modelling tools based on the assumption of lithosphere extension are used to extract this information.

However, lithosphere extension models do not satisfactorily explain the evolution of complex rift systems such as volcanic passive margins, thereby giving erroneous stretching factors β . Notably, they fail to reproduce key observations at the outer parts of volcanic margins including uplift at the time of the breakup, the massive occurrence of mafic extrusive known as seismically identified seaward dipping reflectors (SDRs) and a lower crustal body (LCB) interpreted as magmatic underplating (Holbrook et al., 2001; White et al., 1987), highly intruded lower crust (Abdelmalak et al., 2017; White et al., 2008), or granulite/eclogite lower crustal rocks related to the Caledonian orogeny (Gernigon et al., 2006). In addition, these models fail to explain the high vitrinite values and the presence of LCB below hyper-extended basins at the central parts of volcanic margins although they generally succeed at explaining the subsidence history (Fjeldskaar et al., 2008; Theissen & Rüpke, 2009; Theissen-Krah et al., 2017). Additional processes are, hence, required to reproduce the key observations at volcanic passive margins (Figure 1).

In the North Atlantic region, authors have proposed the arrival of the hot Icelandic mantle 'plume' (Skogseid et al., 2000) as the mechanism causing excess magmatism and uplift at the time of the breakup. Others instead propose independent sub-lithospheric processes such as small-scale convection (SSC, Meyer et al., 2007; Petersen et al., 2018; Simon et al., 2009; van Wijk et al., 2001).

Additional uplift could also result from mantle phase transitions caused by pressure and temperature changes in the mantle during extension (Kaus et al., 2005; Simon & Podladchikov, 2008). The retention of low-density melt in the asthenosphere before breakup has been proposed to explain uplift at the outer parts of passive margins (Quirk & Rüpke, 2018).

Highlights

- We propose new models for the evolution of the multirift Vøring Volcanic Margin.
- Models with an Eocene plume, magmatism, and mantle phase transitions reproduce key observations.
- Models predict the pre-drift margin width evolution.
- The major phases of margin widening are Late Permian and mid-Cretaceous.

At last, standard lithosphere extension models do not include possible serpentinization of the upper mantle. Lundin and Doré (2011) proposed that the serpentinization of the upper mantle below highly extended sedimentary basins is widespread at the North-Atlantic passive margins. The embrittlement of the very thin crust (less than 5-km thickness) below the hyperextended basin in the presence of seawater may cause the serpentinization of the peridotite and consequently density reduction that can generate uplift and seismic and gravity signals similar to LCBs (Rüpke et al., 2013).

All the aforementioned processes modify the density of the lithosphere; hence, may alter the recorded subsidence leading to different estimates for crustal stretching factors. These processes have been tested separately in the modelling of volcanic margins. Using a backstripping approach, Fjeldskaar et al. (2009) modelled the thermal evolution of the Vøring Margin along a transect crossing the margin. They evaluated the temperature anomaly caused by a hot, massive and instantaneous magmatic underplate emplaced below the Vøring Marginal High at the time of the breakup. Similarly, Theissen-Krah et al. (2017), Cunha et al. (2021), and Gac et al. (2018) have incorporated magmatic underplates in their forward thermal-kinematic models of the Møre Margin, Southern Vøring Margin and Vestbakken Volcanic Margin in the SW Barents Sea, respectively. The approach of these authors is, however, limited because the extent of the magmatic underplate is independent of decompressional melting of the asthenosphere during lithosphere extension. Gernigon et al. (2006) computed the extent of the magmatic underplate directly from the

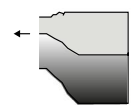
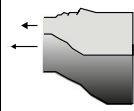
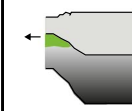
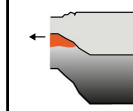
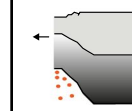
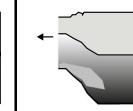
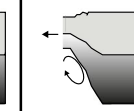

Processes	Pure shear extension	Non-uniform extension	Serpentinization	Magmatic underplate	Melt retention	Phase changes	Small-scale convection	Mantle plume
Lithosphere structure								
Thermal anomaly	positive negative	positive negative	positive negative	positive negative	positive negative	positive negative	positive negative	positive negative
Vertical motion	uplift subsidence	uplift subsidence	uplift subsidence	uplift subsidence	uplift subsidence	uplift subsidence	uplift subsidence	uplift subsidence

FIGURE 1 The tectono-magmatic processes proposed to explain anomalous observations at the outer part of passive margins. The second row from the top illustrates the lithosphere structure associated with each process. The third row from the top illustrates the effect of each process on the thermal structure of the outer margin. Generally, each of these processes causes a hot thermal anomaly beneath the outer margins. The largest thermal anomalies are expected for processes including a mantle plume and/or magmatic underplate. The bottom row depicts the effect of each process on the vertical motion of the outer margin. Lithosphere extensional processes predict subsidence of the outer margin. However, the other processes are expected to produce uplift of the outer margin, with a similar magnitude

volume of magma produced by decompressional melting. They obtained consistent magmatic underplate thickness for models approximating SSC. However, they predict massive, unrealistic underplate thickness for models approximating a plume emplacement. Quirk and Rüpke (2018) did incorporate magmatic processes in the forward thermal-kinematic modelling of the Angola Margin. Melt retention in the sub-lithosphere and magmatic underplate size and geometry is directly computed from the volume of magma produced by decompressional melting of the asthenosphere during extension. Their model reproduces uplift at the time of breakup when melt retention is combined with mantle phase transitions. However, these full magmatic processes have never been simulated in the case of volcanic passive margins characterized by much more voluminous magma production. Aside Quirk and Rüpke (2018), other authors have estimated the contribution of mantle phase transitions to uplift and subsidence (Kaus et al., 2005; Simon & Podladchikov, 2008). However, these models remain largely conceptual. At last, Rüpke et al. (2013) included the serpentinization process in their forward thermal kinematic models of the Vøring Margin to test if the inner LCBs could be of serpentinized mantle origin.

The combined effect of these processes on density and vertical motion has never been evaluated. In this paper, we test new thermal-kinematic models of the well-studied Vøring Volcanic Margin that include consistent magmatic and mantle metamorphic phase transitions. To achieve that a representative crustal transect crossing the Northern Vøring Margin is reconstructed using the

TecMod2D basin modelling suite (Rüpke et al., 2008), we considered two thermal scenarios. In the first scenario, strong mantle stretching and thinning is imposed during the latest Paleocene phase of rifting. Mantle thinning is a simple way to approximate dynamic mantle processes, such as mantle plume emplacement and/or SSC through a kinematic modelling approach. In the second scenario, the mantle lithosphere is thinned later at the late Paleocene-early Eocene time. The contributions of magmatic processes (melt retention and magmatic underplate), deep mantle phase transitions and mantle serpentinization are evaluated. Each model is compared with the whole set of observations along the Vøring Margin in order to identify the best-fit model and the corresponding stretching factors.

2 | THE VØRING MARGIN

The Vøring Margin, part of the mid-Norwegian volcanic passive margin (Figure 2), is bounded by the Jan Mayen Corridor to the southwest and the Bivrost Lineament to the northeast (Blystad et al., 1995; Gernigon et al., 2020). The ca. 500-km-wide Vøring Margin comprises a wide inner domain (Trøndelag Platform), which is bounded to the west by the Halten and Dønna terraces. Further west, the wide central domain is formed by the large and deep Cretaceous Vøring Basin, which is dissected by an elongated boundary fault system of the Fles Fault Complex. The outer part of the Vøring Basin extends to the expected continent-ocean boundaries (COB)

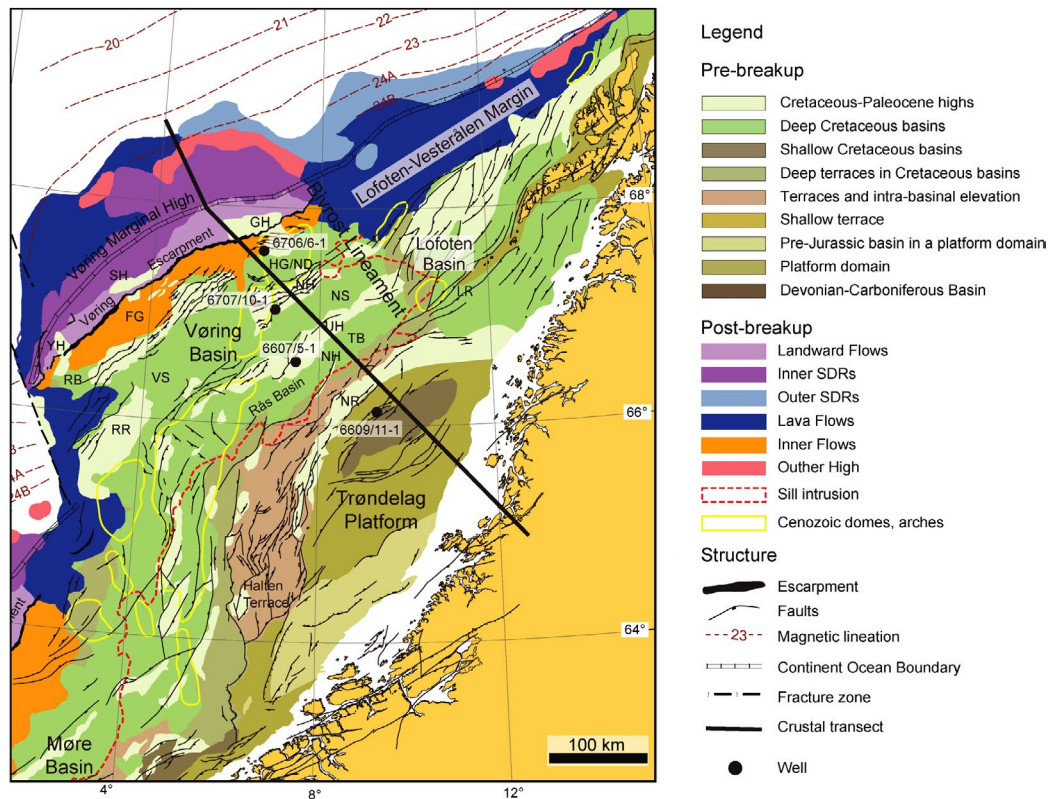


FIGURE 2 Simplified map of the mid-Norwegian margin showing the main tectonic units, fault zones (modified from Abdelmalak et al., 2017) and volcanic seismic facies units (modified from Abdelmalak et al., 2017). FG, Fenris Graben; GH, Grimm High; HG/ND, Hel Graben/Nagfar Dome; NH, Nik High; NR, Nordland Ridge; NS, Någrind Syncline; RB, Rån Basin; RR, Rån Ridge; SDRs, Seward dipping reflectors; SH, Skoll High; TB, Træna Basin; UH, Utgard High; VS, Vigrid Syncline; YH, Ygg High. The MNR11-90698 line for most of the study (Zastrozhnov et al., 2018) ties in with the southern part of the GMNR-94-106C line. The four wells used for the study are shown

through the Vøring Marginal High and represents a series of late Cretaceous-Paleocene structural highs separated by sub-basins.

The Vøring Margin developed through several extensional episodes since the end of the Caledonian orogeny (Figure 3). The early post-orogenic basins developed as large, intra-continental, half-graben systems, controlled by reactivated low-angle detachments such as in the Trøndelag Platform (e.g. Blystad et al., 1995). The main lithospheric extensional events occurred in the late Permian-early Triassic, late Jurassic-early to mid-Cretaceous and late Cretaceous-Paleocene (Brekke, 2000; Eldholm & Grue, 1994; Gernigon et al., 2004; Lundin & Doré, 1997; Zastrozhnov et al., 2020). A possible pre-Permian rift event has also been proposed at the Trøndelag Platform (Blystad et al., 1995). The latter two major episodes resulted in the formation of large sedimentary basins in the Vøring Basin province filled by up to 10–12 km-thick Cretaceous-Paleocene successions (e.g. Faleide et al., 2008; Tsikalas et al., 2012; Zastrozhnov et al., 2018).

The late Cretaceous-Paleocene extensional event led to the breakup at the Vøring Margin in the early Eocene.

During the onset of breakup, significant volumes of flood basalts erupted in the outer Vøring Basin and Vøring Marginal High, which were uplifted to shallow marine/subaerial settings (e.g. Berndt et al., 2001). Outside and below the lava flow domains, seismic observations report voluminous sill complexes intruding pre-breakup sedimentary rocks. The refraction data reveal the existence of a high-velocity LCB (>7 km/s) interpreted as underplated magmatic materials (Holbrook et al., 2001; Kelemen & Holbrook, 1995), or highly intruded lower crust (Abdelmalak et al., 2017; White et al., 2008). The post-breakup evolution of the Vøring Margin is mainly characterized by thermal cooling and regional subsidence of the sedimentary basins (Brekke, 2000; Faleide et al., 2008).

3 | DATA

3.1 | Crustal transect

Our representative crustal transect across the Northern Vøring Margin (Figure 4b) is a composite line comprising

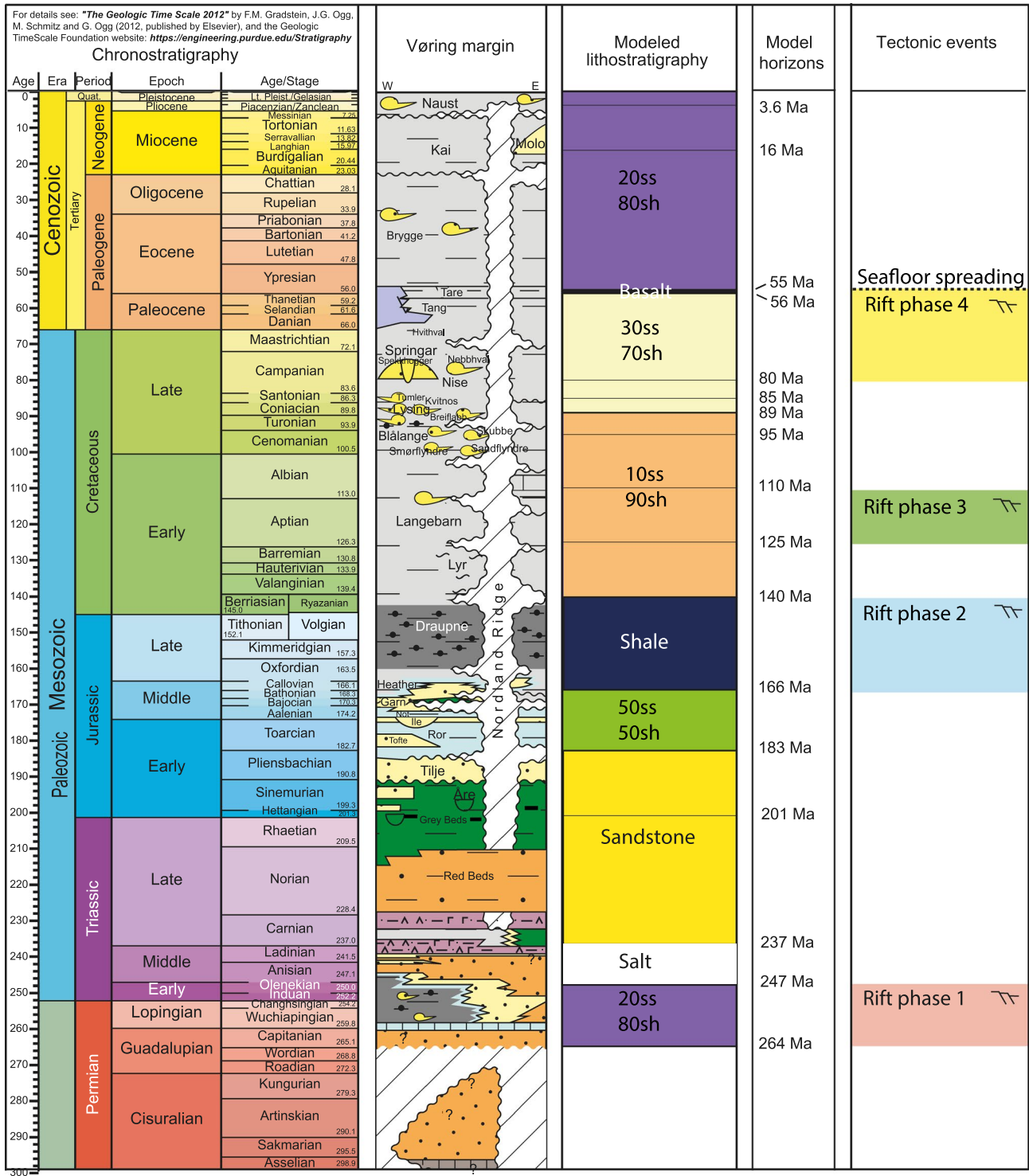


FIGURE 3 Lithostratigraphic column (modified from Gradstein et al., 2010) and main tectonic events for the Northern Vøring Margin. Modelled rift phases are shown in the far right column, spanning the duration of rifting in TecMod2D

two separate seismic reflection profiles: (1) the GMNR-94-106C line for the southern part; and (2) the MNR11-90698 line for the northern part (Zastrozhnov et al., 2018).

The transect runs from the continental shelf to the Vøring Marginal High and images the sedimentary strata in the Vøring Basin and the typical lava flows and SDRs

approaching the continent-ocean boundary in the north-east. At this location, the transition from continental to oceanic crust can also be characterized by lateral velocity changes at mid-crustal and lower crustal levels near the inner edge of the SDRs which is related to a clear density contrast (e.g. Breivik et al., 2009; White & Smith, 2009).

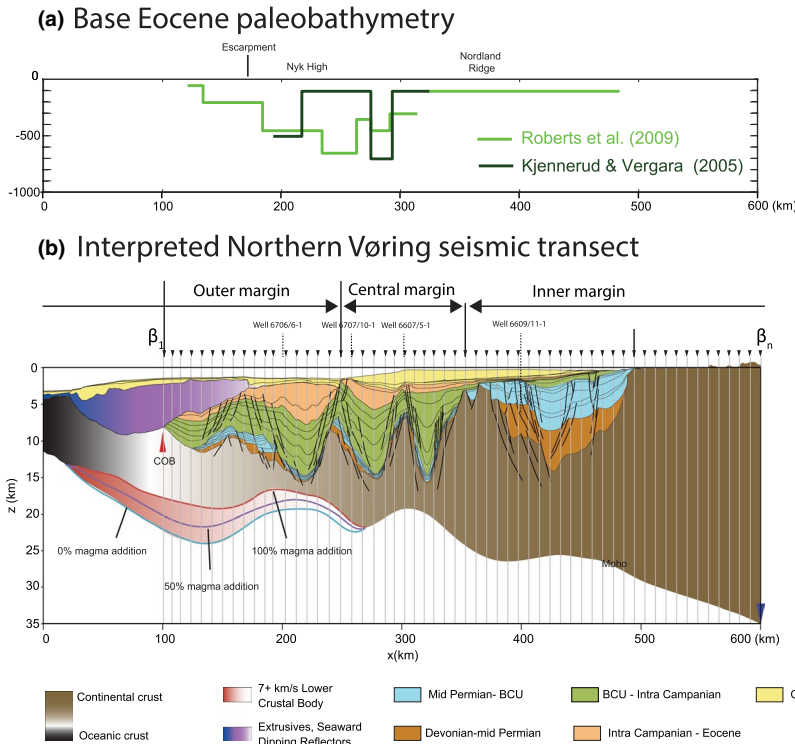


FIGURE 4 The transect crossing the Northern Vøring Margin with (a) paleobathymetry trend along the Northern Vøring transect inferred from Kjennerud and Vergara (2005) (dotted green line), and Roberts et al. (2009) (green line) and (b) the interpreted seismic profile. The margin is sub-divided in inner, central and outer margins (Gernigon et al., 2020)

This profile can be subdivided into inner, central and outer parts where we identify structural highs separating the sedimentary depocentres. The stratigraphic interpretation is based on the interpretation of Zastrozhnov et al. (2018). The deep crustal horizons such as a top basement, top LCB and depth to Moho are extracted from available refraction data in the outer margin (Abdelmalak et al., 2017; Funck et al., 2017; Zastrozhnov et al., 2018) and potential field data (Breivik et al., 2010; Mjelde et al., 1998; Zastrozhnov et al., 2018).

3.2 | Well data

Data from a series of wells drilled in the vicinity of the modelled transect are used to verify and calibrate the models (Figures 2 and 6). The data used include vitrinite reflectance (%Ro) and bottom hole temperature measurements. Well 6706/6-1, well 6707/10-1 and well 6609/11-1 are located within 20 km off the transect, whereas well 6607/5-1 is located over 35-km south-west from the transect.

3.3 | Paleobathymetry

Paleobathymetry is an important parameter that is difficult to quantify. Using biostratigraphic analysis (Ren et al., 2003) and 3D backstripping restoration techniques (Kjennerud & Vergara, 2005; Roberts et al., 2009), authors

proposed paleobathymetry reconstructions for different horizons at the Vøring Margin. The most reliable paleobathymetric reconstruction is for the latest Paleocene-Base Eocene (Figure 4a). Many observations indicate the outer margin was emergent at that time. Subaerial basalt flows and SDRs of the Vøring Marginal High are observed at the Paleocene/Eocene boundary (Berndt et al., 2001), where the escarpment indicates the shoreline position (Abdelmalak et al., 2016). Eastwards the reconstructed paleo water depth is more uncertain, authors suggest basin depths that range from a shallow 100 m (Kjennerud & Vergara, 2005) to deep 200–700 m (Roberts et al., 2009). However seismic interpretation indicates erosion of the Nordland Ridge and Nyk High around the breakup time (Zastrozhnov et al., 2020). The other reconstructed surfaces from the base Cretaceous to base Cenozoic and postbase Eocene are less reliable because there is less primary bathymetric control.

4 | METHODS

4.1 | The inverse modelling approach

TecMod2D is a basin modelling software package that automates sedimentary basin reconstruction in 2D. It is based on an algorithm that couples a forward lithosphere stretching model to an inverse scheme which automatically updates crustal β and mantle δ stretching factors and paleobathymetry until the input stratigraphy is fitted to

desired accuracy (generally within 5%–10% error) (Rüpke et al., 2008, 2010). The 2D forward model is based on pure shear kinematics (McKenzie, 1978) and allows for multiple rifting events of finite duration (Jarvis & McKenzie, 1980). TecMod2D allows also for differential stretching between crust and mantle.

The effects of flexural isostasy and depth of necking are included (Braun & Beaumont, 1989; Watts et al., 1982). The velocity field derived from pure shear kinematics and crustal flexure is used to advect the temperature field. The time-dependent heat-transport equation includes advection and diffusion and is solved in the entire modelling domain.

Crustal radiogenic heat production is assumed to decrease exponentially with depth (Jaupart et al., 1981; Turcotte & Schubert, 2002). Water and sediments are included in the thermal solver to account for the effects of sediment blanketing (Theissen & Rüpke, 2009). Sedimentation is controlled by sedimentation rates determined by the inversion scheme. The deposited sediments are compacted using empirical compaction laws (Royden & Keen, 1980; Sclater & Christie, 1980).

The boundary conditions for the thermal solver are fixed temperatures at the base and top of the numerical domain and zero horizontal heat flow at the sides. In the absence of metamorphic phase transitions, density changes are computed from a reference density and the thermal expansion factor (McKenzie, 1978).

4.2 | Model setup

The stratigraphic section is an interpretation of the Northern Vøring transect (Figure 4b) published in

Zastrozhnov et al. (2018). The section was loaded into TecMod2D for analysis. Rock properties were assigned to each stratigraphic layer (Table 1). Assumptions regarding the lithology of each unit were made, choosing either the dominant lithology (e.g. sandstone) or mixtures (e.g. 50% sand, 50% shale). Likewise, porosity-depth trends linked to mechanical compaction during burial were applied to each rock unit based on the assumed dominant lithology, whereas sand-shale mixtures were linearly interpolated based on their ratios. For simplicity, chemical compaction, diagenesis, and low-grade metamorphism were neglected.

We assume that the first main rift episode took place in the late Permian-early Triassic. Hence, four main rifting phases were defined in our model setup: late Permian-early Triassic (264–247 Ma), late Jurassic-early Cretaceous (166–140 Ma), mid-Cretaceous (125–110 Ma), and late Cretaceous-Paleocene (80–56 Ma).

Model input parameters are summarized in Table 2. Flexural isostasy is applied through an effective elastic thickness (T_e) of 2 km and a corresponding necking depth of 15 km. These values are difficult to constrain and vary spatially and temporally but are consistent with other published models for the Viking Graben and Vøring Basin (Fjeldskaar et al., 2004, 2009; Rüpke et al., 2008; Theissen & Rüpke, 2009).

Post-Caledonian crust and lithosphere varied in thickness along the profiles before rift initiation, but this geometry is unknown. The constant initial crustal thickness of 35 km (17.5 km upper crust, 17.5 km lower crust) and a total lithospheric thickness of 120 km are, therefore, used for most of our models (Clark et al., 2014; Gac et al., 2018; Theissen & Rüpke, 2009). Two of our

TABLE 1 Rock properties assigned to the basin infill within the basin models for the Northern Vøring transect

Lithology	Density (kg/m ³)	Thermal exp. (1/K)	Rad. heating (W/m ³)	Heat capacity (J/kg/K)	Grain cond. (W/m/K)	Porosity	Inv.comp. length (1/km)
Water	1000	0	0	4000	0.65	0	0
Peridotite	3340	3.2E–05	0	1000	3.5	0	0
Basalt	2600	0	1E–07	1000	2	0	0
U. crust (granite)	2850	2.4E–05	2.5E–06	1000	3	0	0
L. crust (diabase)	2900	2.4E–05	2.5E–06	1000	3	0	0
Sandstone	2690	0	1E–06	1000	4.4	0.4900	0.27
Shale	2720	0	1E–06	1000	1.5	0.6200	0.50
10ss90sh	2717	0	1E–06	1000	1.6704	0.6200	0.49
20ss80sh	2714	0	1E–06	1000	1.8602	0.6000	0.46
30ss70sh	2711	0	1E–06	1000	2.0716	0.5900	0.44
50ss50sh	2705	0	1E–06	1000	2.5690	0.5600	0.39
60ss40sh	2702	0	1E–06	1000	2.8609	0.5500	0.37
Salt	2300	4.4E–5	0	1000	4	0.05	0

Model parameter	Value	Units
Forward parameters		
Lithosphere thickness	120	km
Upper crust	17.5	km
Lower crust	17.5	km
Top and bottom temperature	0 and 1300	°C
e-fold length radiogenic heating (crust)	20	km
e-fold length correction	$f(\text{crust})$	
Matrix conductivity	$f(T)$	W/m/K
Pore fluid conductivity	0.6	W/m/K
Effective conductivity	Geometric	W/m/K
Numerical resolution of finite element mesh (nx/ny)	100/100	
Effective elastic thickness (T_E)	2	km
T_E boundary conditions—left	2	km
T_E boundary conditions—right	2	km
Necking depth	15	km

TABLE 2 Input physical forward parameters and inversion control parameters used in this study. These parameters are the same for all modelled scenarios

models possesses an initial 33-km-thick crust (16.5 km upper crust, 16.5 km lower crust) and 87-km-thick mantle lithosphere.

Other main forward model parameters include temperature boundary conditions of 0°C at the seafloor, and 1300°C at the lithosphere-asthenosphere boundary (LAB) and a $2 \mu\text{W}/\text{m}^3$ radiogenic heat production in the crust. The numerical resolution of the finite element mesh is set at $n_x = 100$ and $n_y = 100$.

4.3 | Two thermal scenarios

The late Paleocene-early Eocene emplacement of a mantle plume and SSC during the last late Cretaceous-Paleocene rifting event have been proposed to explain the outer margin anomalies.

The breakup in the NE Atlantic is believed to be linked to the arrival of the Iceland plume (Skogseid et al., 2000), as an explanation of the large igneous activity with flood basalts that created the Vøring Marginal High and up to a 70-km-wide extrusive complex. Uplift, erosion and underplating of the western part of the margin are all associated with the breakup. According to conceptual models, the initiation of magmatism in the North-Atlantic region at 62–63 Ma is contemporaneous with the impingement of the Iceland plume beneath the Greenland lithosphere (Lawver & Müller, 1994; Skogseid et al., 2000). The thermal anomaly associated with the plume head spreads laterally resulting in surface uplift over large areas (Skogseid et al., 2000). Griffiths and Campbell (1990) estimated a c. 100°C thermal anomaly associated with the plume head.

Skogseid et al. (2000) predicted a ca. 1 km uplift of areas located along the rift zone, including most of the mid-Norwegian margin.

Sub-lithospheric processes have been proposed to explain magmatism and uplift at rifted margins without the need for an anomalously high mantle temperature (van Wijk et al., 2001). Such processes include foremost SSC triggered by rifting (e.g. Boutilier & Keen, 1999; Simon et al., 2009). Mutter et al. (1988) first suggested that SSC induced by lateral temperature gradients may provide an enhanced flux of material into the region of partial melting, thereby increasing magmatic activity in the absence of high mantle potential temperatures. In addition, convection increases the amount of heat transported vertically into the rift and laterally out of it significantly amplifying the uplift of rift shoulders (Buck, 1986). The mantle flow associated with a SSC mechanism results in mantle locally thinning more than the crust (Buck, 1986; Huisman et al., 2001).

Unfortunately, it is difficult to simulate these dynamic processes through a kinematic modelling approach. Hence, mantle thinning is imposed to approximate the thermal anomaly created by these mantle processes. Two thermal scenarios are considered.

4.3.1 | Mantle stretching and thinning during the latest late Cretaceous-Paleocene rifting event

We impose a mantle stretching factor larger than the crustal stretching factor during the last, late Cretaceous-Paleocene

rifting event. The pronounced mantle stretching allows to approximate (1) the heat provided by mantle processes added to (2) the pure shear stretching and upwelling of the mantle asthenosphere occurring because of lithosphere extension (McKenzie, 1978). The mantle stretching factor is set to 5 beneath the SDRs and progressively reduces down to 1 at the inner edge of the SDRs. This large mantle stretching factor effectively simulates the production of a large enough amount of magma to give a few km thick underplate.

4.3.2 | Mantle thinning and mantle plume emplacement at the breakup time

The thermal anomaly caused by mantle processes is simulated by imposing a thinning of the mantle lithosphere from 56 to 54 Myr. The mantle lithosphere thins by a factor of 2.5 on the western side of the transect and progressively decreases down to 1 at the inner edge of the SDRs, near the east end of the Hel Terrace.

4.4 | Additional processes

4.4.1 | Melt retention

Quirk and Rüpke (2018) hypothesize that the relative impermeability of mantle lithosphere to melt may be the root cause of additional elevation before the breakup. Thus, as continental plate thins during rifting, the asthenosphere wells up and pressure is reduced causing it to partially melt in proportion to the height the asthenosphere rises. Melt has a lower density than the parent asthenosphere and will tend to migrate upwards through the asthenosphere by compaction once a percolation threshold defined by melt-filled porosity is crossed. However, the overlying mantle lithosphere acts as a barrier, impeding its upward flow leading to the accumulation of melt in the asthenosphere making it buoyant so that the overlying lithosphere rises leading to additional uplift. When the rifting plate breaks, the melt is then expelled to the embryonic ocean ridge as seafloor spreading starts.

TecMod2D implements melt generation based on a simple parameterization of melting as well as melt retention and extraction. Melt production starts once the LAB rises above 90-km depth. It achieves maximum value at 20 km depth. Melt fractions are linearly interpolated between these two reference points. A specified fraction of melt is emplaced as a magmatic underplate. During the post-rift, the melt is extracted from the asthenosphere at a specified rate.

4.4.2 | Mantle phase transitions

The phase transitions of dry mantle peridotites have been proposed to explain surface vertical motions (Kaus et al., 2005; Simon & Podladchikov, 2008). Under varying pressure and temperature conditions, dry peridotite experiences phase transitions associated with significant density jumps. Authors proposed late syn-rift uplift observed at rifted margins is caused by phase transitions, such as garnet-spinel and plagioclase-spinel, that take place during basin formation (Kaus et al., 2005; Petrini et al., 2001; Podladchikov et al., 1994; Simon & Podladchikov, 2008; Yamasaki & Nakada, 1997). The garnet-spinel peridotite transition leads to a moderate decrease in density of the mantle part of the lithospheric column at the initial stages of stretching. Then, when the crust is sufficiently thinned and the temperature is relatively high, the plagioclase-in reaction causes a strong density reduction of the upper mantle. The formation of plagioclase peridotite can explain syn-rift uplift in sedimentary basins that experienced large mantle stretching without invoking an unrealistically strong increase in temperature. It might also be responsible for the prebreak-up unconformity observed at continental margins (Simon & Podladchikov, 2008). TecMod provides thermodynamic tables of mantle densities based on mantle phase transition models from Kaus et al. (2005) and Simon and Podladchikov (2008) for various mantle compositions (Hartz et al., 2016).

4.4.3 | Mantle serpentization

Serpentinization is the transformation of a dry peridotite to a wet serpentinite in presence of seawater at temperatures ranging from 500 to 600°C (Skelton et al., 2005). The transformation of a dry peridotite to a wet serpentinite involves a density reduction and a significant decrease in seismic velocities implying that a partially serpentized mantle can have seismic and gravity signals similar to LCBs. Deserpentinization can occur if serpentized rocks move out of their thermal stability field.

TecMod can simulate mantle serpentization processes during rifting. For serpentization to occur, crustal-scale brittle faulting is necessary to provide pathways for seawater to reach and react with mantle rocks. Hence, TecMod tracks the rheological evolution of the extending lithosphere. The entire crust needs to be brittle implying that the brittle yield stress is everywhere lower than the ductile yield stress. The brittle yield stress is controlled by Bylerlee's law (Ranalli & Murphy, 1987). The ductile yield stress is computed from viscous flow laws. The details of the implementation can be found in Rüpke et al. (2013).

4.5 | The quest for the best-fit model

The best-fit model must reproduce the key observations at both the inner margin and the outer margin: (1) the observed stratigraphy (subsidence), (2) the observed beta factors along the transect, (3) the vitrinite reflectance, notably the high %Ro values observed at the outer margin, (4) the base Eocene paleobathymetry along the transect, marked by an emergent outer margin and some structural highs, and (5) the interpreted magmatic underplate below the outer margin.

Numerous models were run. The two thermal scenarios, mantle thinning during or after the latest rifting event were modelled. Variations of the two scenarios, including either magmatism or mantle phase transitions or both, were studied. For each model, we evaluated the effects of the main controlling parameters, such as the initial crustal thickness (from 30 to 40 km), local versus regional isostasy, and the number of rifting events. In all, hundreds of models were calculated. For each model, the computed %Ro, the base Eocene paleobathymetry, and magmatic underplate geometry are compared to the observations until best-fit models are identified. We choose to show the relevant ones in the paper.

5 | RESULTS

After presenting a standard reference model (named 'Ref'), we model the two scenarios for the evolution of the Vøring margin. In the first scenario (models named 'SSC'), a strong mantle stretching factor is imposed during the late Cretaceous-Paleocene rifting event. In the second scenario (models named 'Plume'), we imposed a thinned mantle lithosphere at the breakup time between 56 and 54 Ma. Variations of each scenario are tested. These models are run with an initial 35-km-thick crust. Thereafter, two additional standard models are run with an initial 33-km-thick crust, the second one including serpentinitization (Table 3).

5.1 | Model Ref—Reference model

The automated basin reconstruction across the Northern Vøring transect is presented in Figure 5. The convergence of the modelled stratigraphy to the input stratigraphy is good (approximately 5%) after 20 iterations.

Vitrinite reflectance (%Ro), bottom hole temperature and drill stem test (DST) temperature measurements were acquired for 4 wells within 35 km of the transect (Figure 2 for well locations). The %Ro measurements are plotted against the modelled %Ro trends and the temperature measurements are plotted against the modelled geotherms (black line on Figure 6b,c). Well control points show a good correlation when comparing against the bottom hole and DST temperatures. The vitrinite reflectance values show a good correlation for wells located on the inner margin (well 6607/5-1 and well 6609/11-1), as indicated by the low mean absolute percentage error (MAPE, less than 15%, Figure 6a). However, the correlation is poorer for the wells located at the outer margin, especially at the outermost well, well 6706/6-1, as indicated by the larger MAPE (more than 30%, Figure 6a).

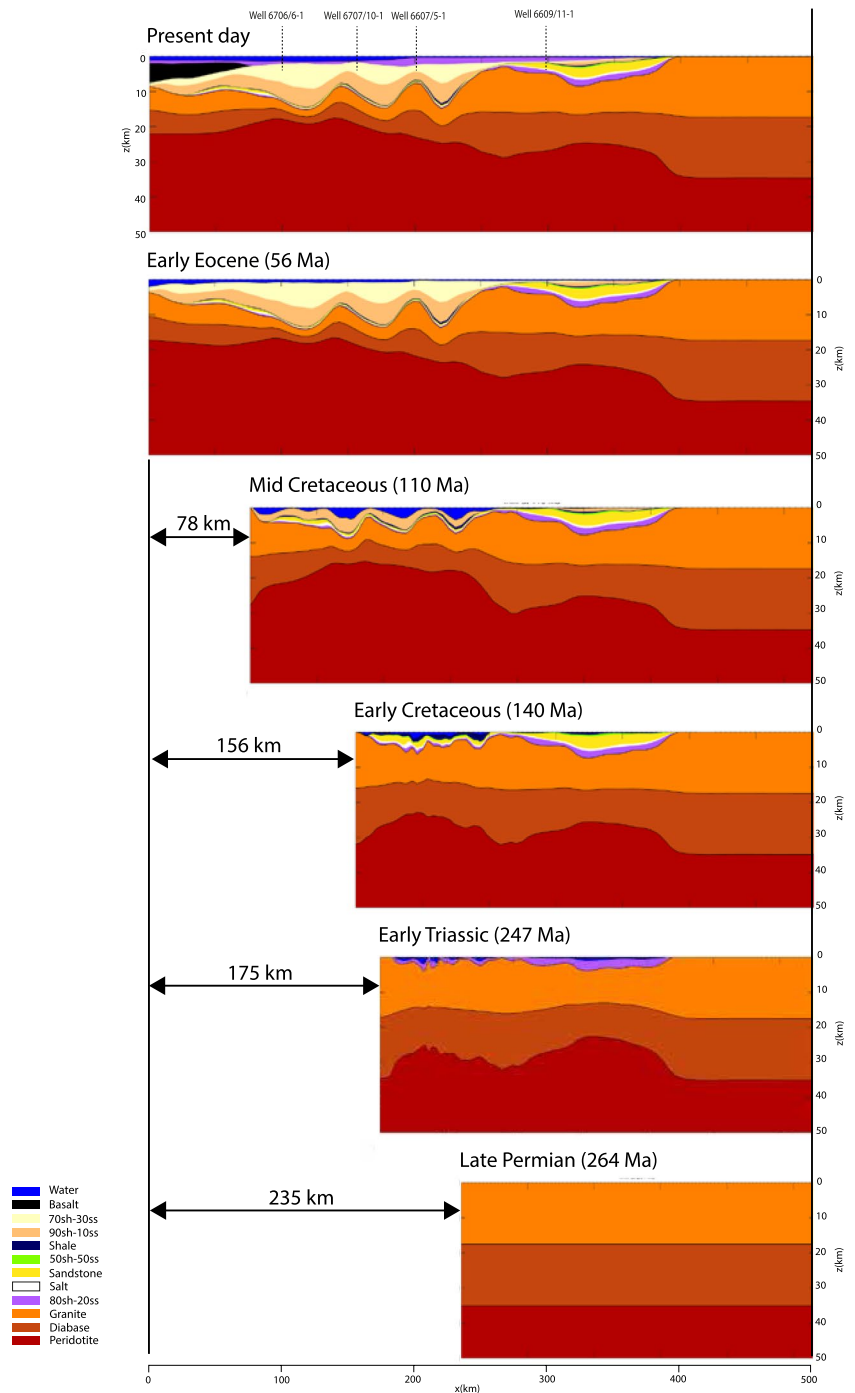
A maximum cumulative β factor of 9 is modelled over the deep Hel Graben (Figure 7a). Maximum stretching occurs during the mid-Cretaceous rifting phase (Figure 7b), the stretching is focused over the Hel Graben, Någrid Syncline and Træna Basin and is absent further east. A regional trend can be seen in the β -factor distributions, with the main axis of extension roughly migrating westward until the Paleocene. The Trøndelag Platform was the main focus of extension during the Permian (Figure 7b).

The modelled cumulative crustal stretching factor β is compared to the stretching factors inferred from the observed crustal thinning (in the rest of the manuscript we name it 'observed stretching factor'). The thinning factor is estimated for three LCB interpretations (whereby the LCB is made of 0%, 50% and 100% magmatic material). It is the ratio between the observed crustal thickness and a reference crustal thickness. The observed crustal thickness is measured from the top Permian horizon to the seismic Moho.

Model	Description
Ref	Reference model
SSC	Small-scale convection
SSCMelt	Small-scale convection, magmatic processes
Plume	Eocene plume
PlumeMelt	Eocene plume, magmatic processes
PlumeMeltPT0	Eocene plume, magmatic processes, mantle phase transitions
PlumeMeltPT1	Same as PlumeMeltPT0 with heterogenous crust
Ref33	Reference model, 33-km-thick crust
Ref33Serp	Mantle serpentinitization, 33-km-thick crust

TABLE 3 The different models

FIGURE 5 Modelled cross-sections along the Northern Vøring Margin at different time steps from the late Permian to Present-day for the reference model Ref



We consider a 35-km thickness for the reference continental crust (Gernigon et al., 2006; Theissen & Rüpke, 2009). The observed stretching factor is marked by three peaks localized over the three basins, the Hel Graben, the Någrind Syncline, and the Træna Basin (green line on Figure 8a). The observed stretching factor over the Hel Graben depends on the interpreted LCB: It is ca. 8 for a 0% magmatic LCB and ca. 20 for a 100% magmatic LCB. The observed stretching factor achieves almost 5 over the easternmost deep basins (the Någrind Syncline and the Træna Basin). The cumulative crustal stretching factor β modelled for the reference

model Ref agrees well with the observed stretching factors for a ca. 0% magmatic interpreted LCB (Figure 8a).

Computed paleobathymetry along the transect (black line on Figure 8b) is compared with the interpreted paleobathymetry at the base Eocene, the most reliable time period (green line on Figure 8b). In general, the pure shear reference model Ref predicts a too cold outer margin mantle evolution leading to water depths deeper than observations. The discrepancy is modest (ca. 200 m) over the Trøndelag Platform but up to 1000 m over the Hel Terrace.

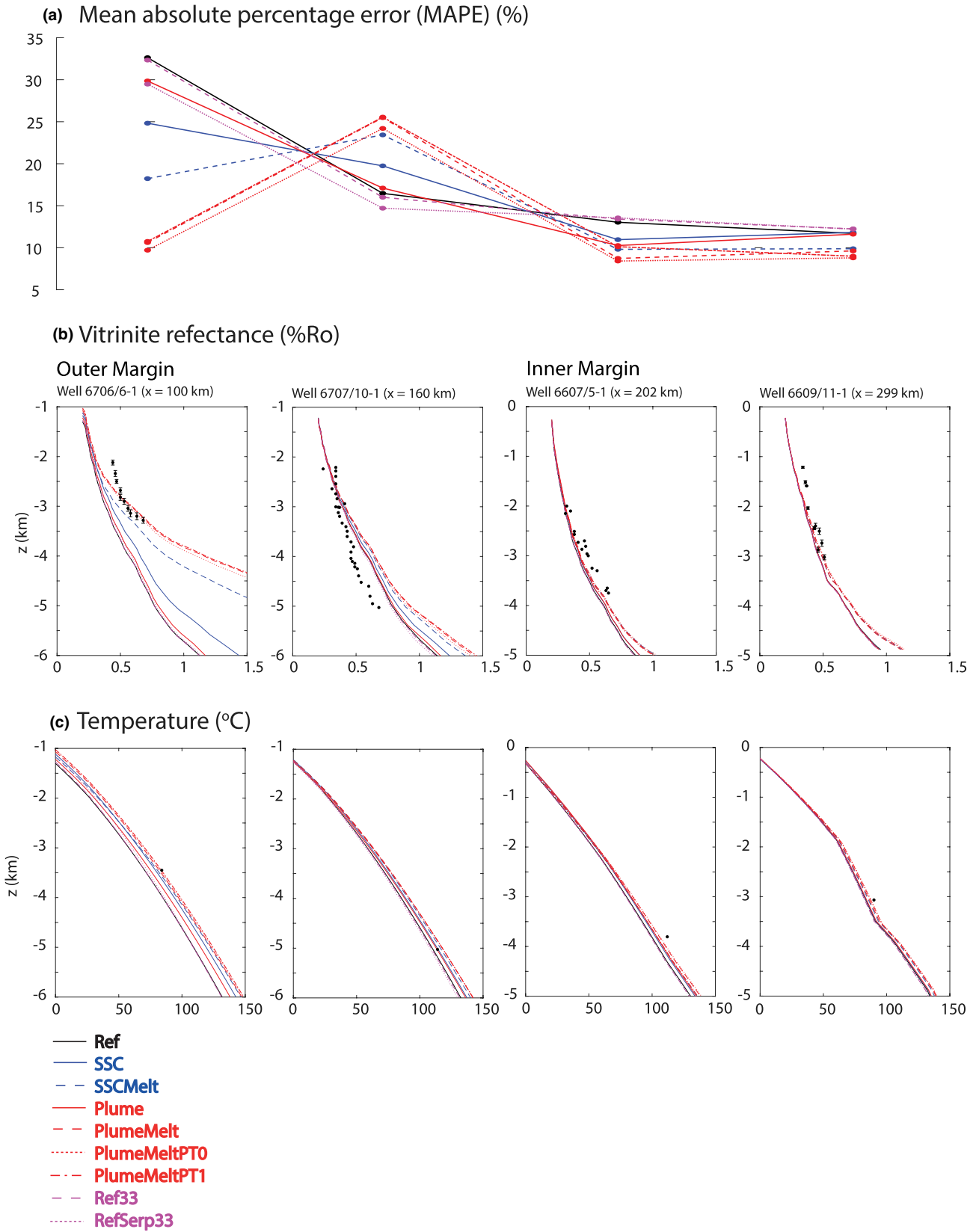
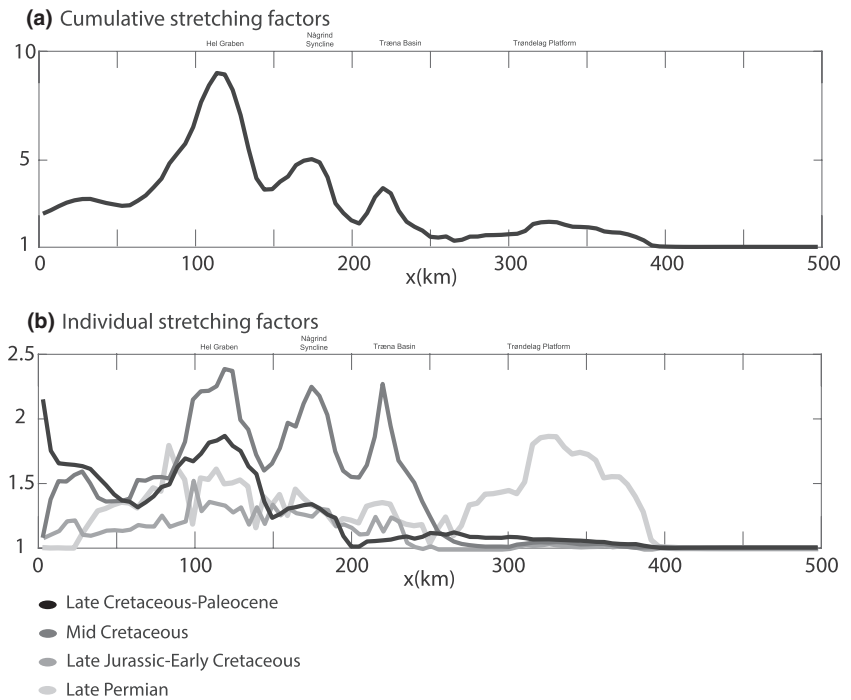


FIGURE 6 Quality control for the models. The sketches show (a) the mean absolute percentage error between the observed and modelled vitrinite reflectance for the four wells, (b) modelled vitrinite reflectance %Ro are plotted against measured vitrinite %Ro and (c) modelled temperature are plotted against bottom hole temperature data for each well. For well location see Figure 2

FIGURE 7 Crustal stretching factors (β -factors) calculated along the Northern Vøring profile for the reference model Ref with (a) the cumulative β -factor calculated along the transect and (b) the computed β -factor for the individual modelled rift phases



5.2 | Models SSC with imposed differential crust-mantle stretching during the last rifting event

This series of models examine the effect of forced depth-dependent stretching below the outer margin during the late Cretaceous-Paleocene rifting event on crustal stretching factors, vitrinite reflectance and paleobathymetry.

5.2.1 | Model SSC—Differential stretching, no melt

The model SSC is the same as model Ref except for the differential stretching is set on. The mantle stretching factor is forced to be 5 below the outer margin during the late Cretaceous-Paleocene rifting event. This is much larger than the crustal stretching factor (5 vs. ca. 1.5). Like for reference model Ref, the four well control points show a good correlation for temperature (blue line on Figure 6c). The modelled vitrinite show a good correlation with observed vitrinite at the inner margin (blue line on Figure 6b), the mean absolute percentage error is indeed low, less than 12% (blue line on Figure 6a). At the outer margin, the correlation remains poor; it is a bit improved at well 6706/6-1 compared to model M0 but it is a bit worse at well 6707/10-1 (blue line on Figure 6a).

The modelled cumulative crustal stretching factor β generally reproduces well the pattern of observed stretching factors for a 0%–50% magmatic interpreted LCB (blue line on Figure 8a). Model SSC predicts a peak stretching factor of ca. 10 over the Hel Graben, and a stretching factor

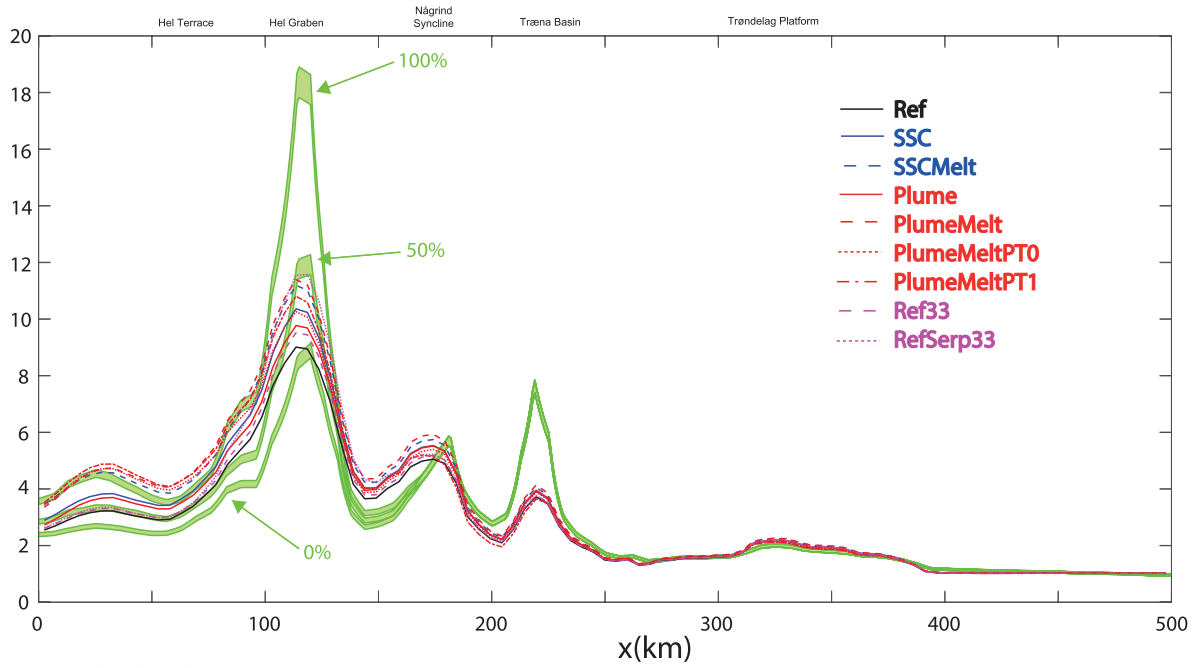
of ca. 5 over the Någrind Syncline in good agreement with the observations.

Like the reference model Ref, the base Eocene-computed paleobathymetry (blue line on Figure 8b) predicts a shallow (ca. 400 m deep) Trøndelag Platform and an emergent Utgard High, in conformity with interpreted paleobathymetry, and a too deep outer margin although the heat supplied by strong mantle stretching partly compensates for the thinning of the crust and gives a slightly shallower Hel Terrace than for model Ref (ca. 800 vs. ca. 1000 m deep).

5.2.2 | Model SSCMelt—Differential stretching, melt

The model SSCMelt is the same as the non-melting model SSC except for melting processes (melt retention and magmatic underplate) are included. Melt retention and magmatic underplate mostly affect the transect west of the Utgard High. Melting occurs when the mantle lithosphere is thinned enough. This happens during the late Cretaceous-Paleocene rifting event where the mantle thins by a factor 5 below the outer margin. A fraction (25%) of melt accumulates below the crust with a temperature of 1200°C to form the magmatic underplate, whereas residual melt remains in the asthenosphere. The magmatic underplate progressively thickens, layer by layer, as the melt is continuously produced during the hot last rifting event. Melt starts to accumulate at 68 Ma, then the magmatic underplate achieves its maximum thickness at 56 Ma.

(a) Modelled crustal stretching factor β and observed thinning factor



(b) Paleobathymetry at Base Eocene (54 Ma) (m)

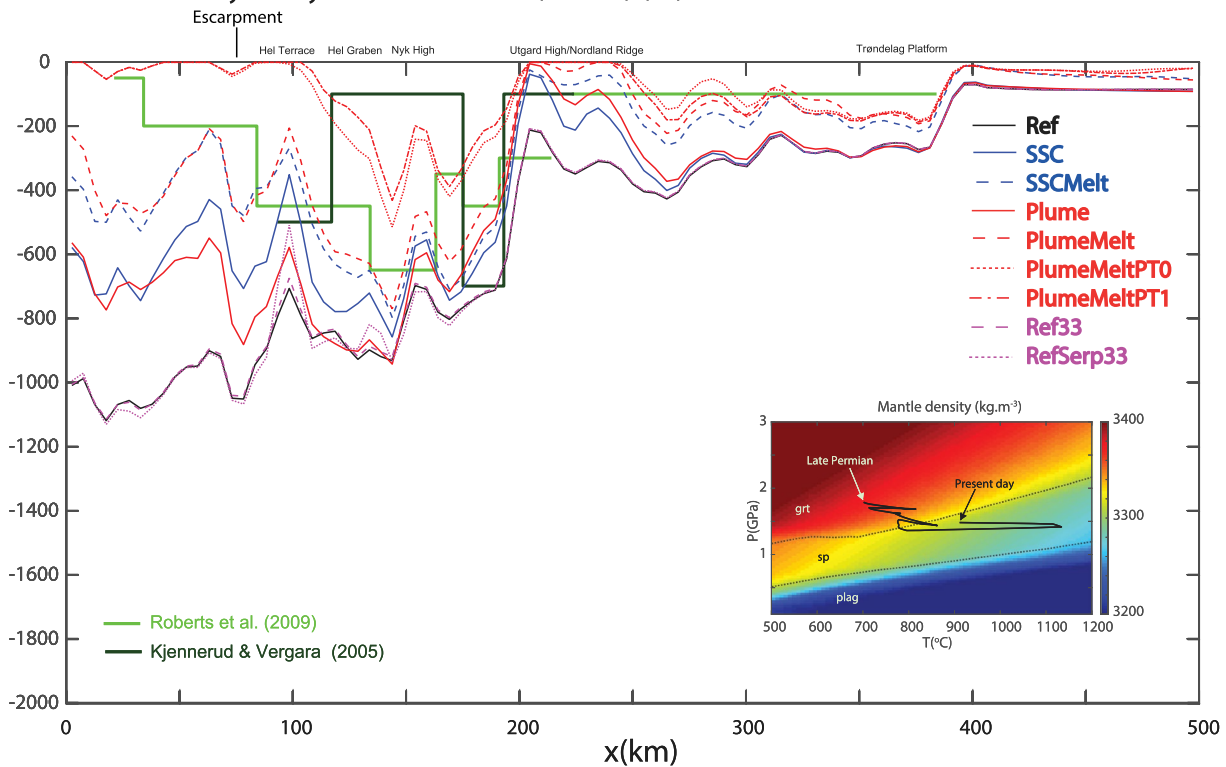


FIGURE 8 Modelled stretching factors and paleobathymetry. (a) Cumulative crustal stretching factors (β -factors) calculated along the Northern Vøring profile for the different models. The green line represents the observed crustal thinning factors for LCB with different magmatic additions (0%, 50% and 100%), (b) Modelled paleobathymetry for the different models along the Northern Vøring profile at the base Eocene (54 Ma). The light green line and the dark green line represent the interpreted paleobathymetry trend extracted, respectively, from Roberts et al. (2009), and Kjennerud and Vergara (2005). The mantle phase transitions and density changes occurring during the model PlumeMeltPT0 evolution are shown in the insert. The black line represents the path followed by a drop of mantle located deep below the outer margin. grt, garnet, sp, spinel, plag, plagioclase

The four well control points still show a good correlation for temperature (dashed blue line on Figure 6c). Modelled and observed vitrinite reflectance %Ro correlate well at the inner margin (dashed blue line on Figure 6b). At the outer margin, the emplacement of hot magmatic underplate leads to higher %Ro values than for non-melting model SSC giving better agreement with the observed vitrinite at well 6706/6-1, as indicated by the lower, ca. 18% versus 25%, MAPE (dashed blue line on Figure 6a). In the same way, at well 6707/10-1, the modelled vitrinite is higher than that for model SSC, but there it leads to a worsened fit with data.

Like for the previous model SSC, the modelled cumulative crustal stretching factor β generally reproduces well the pattern of observed stretching factors for a 0%–50% magmatic interpreted LCB (dashed blue line on Figure 8a). However, the modelled crustal stretching factor is a bit higher at the outer margin (11 over the Hel Graben vs. 10 for SSC) because the crust requires to be stretched more to compensate for the less-dense-than-mantle magmatic underplate.

Model SSCMelt exhibits a similar base Eocene paleobathymetry (dashed blue line on Figure 8b) as the non-melting model SSC: A reasonably shallow Trøndelag Platform and emergent Utgard High, but a too deep outer margin west of the Utgard High although the retention of melt in the asthenosphere during the last rifting event contributes to a ca. 100 m shallower Hel Terrace.

5.3 | Models Plume with late Paleocene-early Eocene mantle thinning

These models look at the effect of a mantellic thermal anomaly emplaced between 56 and 54 Ma on crustal stretching factors, vitrinite reflectance and paleobathymetry. The thermal anomaly is simulated by imposing a 2-Myr-long mantle lithosphere thinning event between 56 and 54 Ma, at the breakup time.

5.3.1 | Model Plume—Late Paleocene-early Eocene mantle thinning, no melt

Model Plume is the same as reference model Ref except for the presence of the thermal anomaly. Like for model Ref, the four well control points show a good correlation for temperature (red line on Figure 6c). Again, at the inner margin, the modelled vitrinite fits well the observed vitrinite reflectance %Ro, the MAPE is indeed very low, less than 10% (red line on Figure 6a,b). However, at the outer margin, the modelled vitrinite remains too low at well 6706/6-1 (MAPE is ca. 30%) and too high for well 6707/10-1 (red line on Figure 6b).

The modelled cumulative crustal stretching factor β generally reproduces well the pattern of observed stretching factors for a 0%–50% magmatic interpreted LCB (red line on Figure 8a). The peak stretching factor is ca. 10 over the Hel Graben, and a stretching factor of ca. 5 is modelled over the Någrind Syncline in good agreement with the observations.

Like the reference model Ref, the base Eocene computed paleobathymetry (red line on Figure 8b) predicts a reasonably shallow (ca. 400 m deep) inner margin but a too deep outer margin although the heat supplied by the pronounced thinning of mantle lithosphere between 56 and 54 Ma gives a shallower Hel terrace than for model Ref (ca. 700 vs. ca. 1000 m deep).

5.3.2 | PlumeMelt—Late Paleocene-early Eocene mantle thinning, melt

The model PlumeMelt is the same as the non-melting model Plume except for melt retention and magmatic underplate are included. Like for model SSCMelt, melt retention and magmatic underplate mostly affect the transect west of the Utgard High. Hot melt accumulates below the Moho to form a ca. 3 km-thick magmatic underplate.

The four well control points still show a good correlation for temperature (dashed red line on Figure 6c). Modelled and observed vitrinite reflectance %Ro correlate well at the inner margin (dashed red line on Figure 6b). At the outer margin, the emplacement of hot magmatic underplate leads to higher %Ro values than for the non-melting model Plume. This gives better agreement (MAPE is ca. 10%, Figure 6a) with the observed vitrinite at well 6706/6-1 but at a level deeper than 2.5 km. In the same way, at well 6707/10-1, the modelled vitrinite is higher than for model Plume, but there it leads to a worsened fit with data.

The modelled cumulative crustal stretching factor β generally reproduces well the pattern of observed stretching factors for a 50% magmatic interpreted LCB (dashed red line on Figure 8a). The modelled crustal stretching factors are higher than for the non-melting model Plume at the outer margin because the crust must be stretched more to compensate for the less-dense-than-mantle magmatic underplate. The peak stretching factor over the Hel Graben achieves 11.

Model PlumeMelt exhibits a similar base Eocene paleobathymetry (dashed red line on Figure 8b) as the non-melting model Plume: a reasonably shallow Trøndelag Platform and emergent Utgard High, but a still too deep outer margin west of the Utgard High. However, the retention of melt in the asthenosphere during the last rifting event contributes to a ca. 200 m shallower outer margin than model Plume.

5.3.3 | Model PlumeMeltPT0—Late Paleocene-early-Eocene mantle thinning, melt, mantle phase transitions

The model PlumeMeltPT0 is the same as the melting model PlumeMelt except for mantle phase transitions are now included. Like for the magmatic processes, phase transitions mostly affect the deeper mantle below the outer margin during the late Paleocene-early Eocene mantle thinning. Heat supplied by the successive rifting episodes than the early Eocene thermal anomaly causes extensive but temporary phase transitions from dense garnet to lighter spinel in the lower lithosphere (see insert on Figure 8b).

The four well control points still show a good correlation for temperature (dotted red line on Figure 6c). Modelled and observed vitrinite reflectance %Ro correlate well at the inner margin (dotted red line on Figure 6b). At the outer margin, for the same reasons as the previous model PlumeMelt, model PlumeMeltPT0 shows good agreement with the observed vitrinite deep at well 6706/6-1 at a deep level and a bad fit at well 6707/10-1.

The modelled cumulative crustal stretching factor β generally reproduces well the pattern of observed stretching factors for a 0%–50% magmatic interpreted LCB (dotted red line on Figure 8a). A maximum cumulative β factor of ca. 10 is modelled over the deep Hel Graben (dotted red line on Figure 8a).

This model shows a general good fit with paleobathymetry data. The computed paleobathymetry (dotted red line on Figure 8b) is markedly different from the previous models west of the Utgard High. Model PlumeMeltPT0 predicts a ca. 600 m deep Hel Graben followed by a very shallow Hel Terrace, in excellent agreement with the interpreted paleobathymetry trend. The garnet-spinel phase transition in the deeper mantle provides enough density reduction (ca. 50 kg/m³ over a ca. 50-km-thick mantle column) to cause temporary uplift and emergence of the outer margin. East of the Utgard High the trend is similar to previous models, with a few hundred meters deep Trøndelag Platform and subaerial Nordland Ridge, in good agreement with data.

5.4 | 33-km-thick models M0

5.4.1 | Model Ref33—No serpentization, 33-km thick crust

The model Ref33 is the same as reference model Ref except the initial crustal thickness is 33 km (instead of 35 km). Again, all four well control points show a good correlation for temperature (dashed magenta line on Figure 6a). Modelled and observed vitrinite reflectance %Ro correlate well at the inner margin (dashed magenta line on

Figure 6b). However, at the outer margin, like model Ref, model Ref 33 shows poor agreement with the observed vitrinite. The modelled vitrinite is too low at well 6706/6-1 and too high at depth for well 6707/10-1.

The modelled cumulative crustal stretching factor β generally reproduces well the pattern of observed stretching factors for a ca. 0% magmatic interpreted LCB (dashed magenta line on Figure 8a). In general, the modelled crustal stretching factors (dashed magenta line on Figure 8a) are a bit higher than for the 35-km-thick reference model Ref (black line on Figure 8a).

Model Ref33 paleobathymetry (dashed magenta line on Figure 8b) is almost undistinguishable from the 35-km-thick crust reference model Ref. It predicts a westward deepening trend, with a shallow Trøndelag Platform, an emergent Nordland Ridge, and a too deep Hel Terrace.

5.4.2 | Ref Serp33—Serpentization, 33-km-thick crust

The model Ref Serp33 is the same as the previous model Ref33 but mantle serpentization is set on. The 33-km-thick crust model is thin enough to allow for local crustal-scale brittle faulting; hence, water penetrates through the upper mantle.

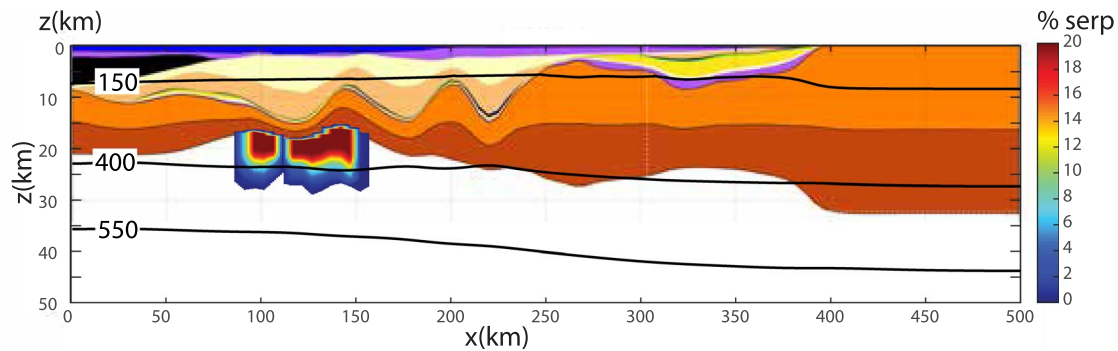
Again, all four well control points show a good correlation for temperature (dotted magenta line on Figure 6c). Modelled and observed vitrinite reflectance %Ro correlate well at the inner margin (dotted magenta line on Figure 6b). At the outer margin, like previous model Ref33, model vitrinite reflectance %Ro is too low at well 6706/6-1 and too high at depth for well 6707/10-1.

Serpentization is confined to the upper mantle below the highly stretched crust from the Hel Graben to the Nyk High (Figure 9). TecMod2D predicts the crust and overlying sediments locally becomes entirely brittle during the mid-Cretaceous rifting event allowing for water to infiltrate the cold upper mantle leading to partial serpentization. The upper mantle below the Vøring Basin is then replaced by less dense partially serpentized mantle material.

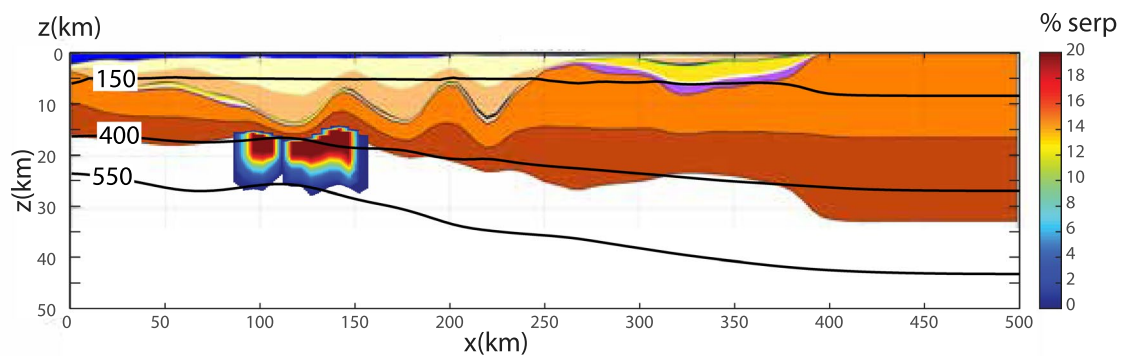
Compared to the non-serpentized model Ref33, model RefSerp33 requires larger crustal stretching factors over the Vøring Basin to compensate for the less-dense partially serpentized upper mantle. The peak stretching factor is ca. 12 over the Hel Graben (compared to ca. 9 for non-serpentized model Ref33), fitting the observed stretching factor for a near 50% magmatic LCB (dotted magenta line on Figure 8a).

Model RefSerp33 (dotted magenta line on Figure 8b) has a very similar base Eocene paleobathymetry trend as the non-serpentized model Ref33. It predicts a reasonably shallow Trøndelag Platform, an emergent Utgard High, and a too deep Hel Terrace.

Present day



Early Eocene (56 Ma)



Middle Cretaceous (110 Ma)

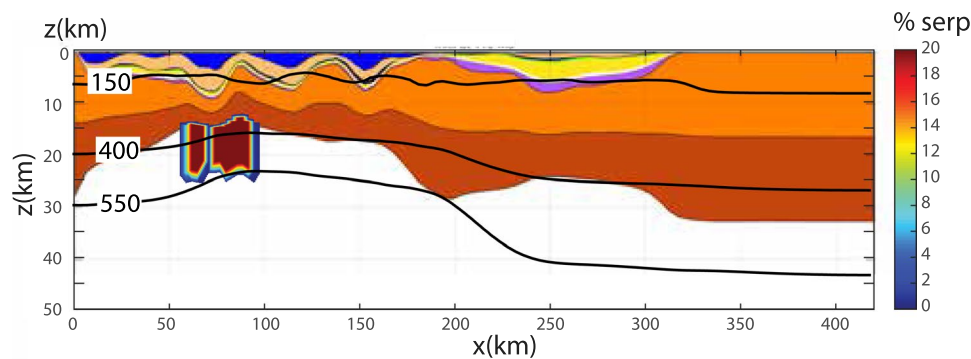


FIGURE 9 Extent of mantle serpentinization for model RefSerp33 at different time steps during the model evolution. Most of the serpentinization occurs between 150 and 400°C. Deserpentinization occurs once rocks move out the thermal stability limit (550°C)

6 | DISCUSSION

6.1 | Summary of results

We have computed 2D thermo-kinematic models of basin evolution based on an inverse-scheme approach to simulate the thermal and tectonic history of the multirift Vøring Margin. The main results are: (1) Standard model

of extension reproduces well the subsidence at the inner part of the Vøring margin, east of the Utgard High but fails to explain the outer margin anomalies, (2) the thermal scenario with strong mantle thinning during the last rifting event and incorporating magmatic processes (melt retention and underplating) satisfactorily explains the LCB with magmatic addition, high vitrinite reflectance values, stretching factors, but predicts a too deep outer

margin, (3) the thermal scenario with mantle thinning at the breakup time and incorporating magmatic processes (melt retention and underplating) and mantle phase transitions satisfactorily explains the magmatic LCB, high vitrinite reflectance values, stretching factors and the emergent base Eocene outer margin and (4) if the initial crust is thin enough (33 km), water can locally penetrate the upper mantle below the highly-extended Vøring Basin triggering a partially serpentinized upper mantle with a seismic and gravity signals similar to LCBs.

6.2 | Model parameters

6.2.1 | Parameter sensitivity

We have chosen reasonable values for the model parameters. However, uncertainties are attached to their value. We have assumed a typical, constant 33/35-km-thick continental crust for the models. However, using a constant initial crustal thickness is simplistic, as the original thickness was unlikely uniform. In addition, the deepest sedimentary rocks can reach diagenesis/low-grade metamorphism pressure and temperature conditions giving P-wave velocities in excess of 5.5 km/s and densities undistinguishable from uppermost crystalline crust rocks. As a consequence, the crustal thickness may be overestimated in places, and the beta factor consequently underestimated.

We have also tested the effect of a colder/warmer lithosphere on modelling results. We run two models with a thinner, 100 km, and thicker, 150 km, lithosphere (vs. 120 km for previous models). We found that the thin lithosphere models predict colder temperature histories leading to smaller vitrinite values, and deeper paleobathymetry for the base Eocene. On the contrary, the thick lithosphere model requires to be stretched much more leading to an unrealistically warm thermal history, very thick underplate, large vitrinite values and shallower paleobathymetry.

At last, we tested models with temperature-dependent elastic thickness. In these models, T_e is controlled by a specific isotherm (usually 450°C roughly corresponding to the brittle/ductile transition) so that the lithosphere strength is temperature-dependent. However, this gives elastic thickness much thicker than suggested by observations. As a consequence, the modelled stretching factors is significantly smaller than that for the 2-km-thick elastic thickness we have used in the previous models.

6.2.2 | Utgard High basement

Seismic and potential field data suggest the presence of a dense lower crustal material beneath the Utgard High

(Zastrozhnov et al., 2018). However, none of the models we have tested can explain the nature of the lower crust there. The models incorporating magmatic processes do not predict a magmatic underplate beneath the Utgard High. Neither can the serpentinized model or RefSerp33 produce a partially serpentinized upper mantle beneath the Utgard High. Hence, it remains that the nature of the lower crust is probably granulite/eclogite.

We have run a variation of the best-fit model PlumeMeltPT0 including a dense crustal body in the lower crust (with a density of 3000 kg/m³, denser than lower crust). The new model is named PlumeMeltPT1. Generally, this heterogeneous model does not differ significantly from the homogeneous model PlumeMeltPT0. The computed vitrinite reflectance (dashed-dotted red line on Figure 6b), paleobathymetry (dashed-dotted red line on Figure 8b) and stretching factors (dashed-dotted red line on Figure 8a) remain similar except for the Utgard High, whereby stretching factors are marginally lower than the homogeneous model, as less stretching is required to assert isostatic balance. Thus, the incorporation of denser lower crustal material below the Utgard High did not affect our results.

6.3 | The outer margin wells 6706/6-1 and 6707/10-1

None of the models satisfactorily reproduce the vitrinite data at well 6706/6-12. Models PlumeMelt, PlumeMeltPT0 and PlumeMeltPT1 reasonably reproduce the vitrinite data at deep levels but they predict too low vitrinite at shallower levels. Additional (near-surface) processes are required to fully reproduce the data. Such processes may include the transport of heat through hydrothermal convection (Cunha et al., 2021; Maystrenko & Gernigon, 2018). Hydrothermal activities have been reported at the Gjallar Ridge (e.g. Njone, 2014; Planke et al., 2005) and indicate that the presence of hydrothermal vent and sill complexes together with accompanying faults could create favourable conditions for local convective heat transfer driven by fluid flow within the north-western part of the Vøring Basin. In addition, the erosion of the upper layers of the subaerial outer margin following the plume emplacement at base Eocene may cause the isostatic uplift of deeper and more mature rocks at shallower levels.

All models predict too large vitrinite values at well 6707/10-1, located on the flanks of the Nyk High. All models predict a too hot thermal history. Models are based on the simple assumption that the basement has a homogeneous composition, presenting the same thermal properties laterally. However, the basement is probably more heterogeneous as suggested by deep seismic data

(Zastrozhnov et al., 2018). Notably lateral variations on radiogenic heat concentrations are to be expected. A less radiogenic crust below the Nyk High may give a colder thermal history leading to smaller vitrinite values, in agreement with the data.

6.4 | Outer margin uplift

The model PlumeMeltPT0, characterized by late Paleocene-Eocene mantle thinning, magmatic processes and mantle phase transitions, best-fits paleobathymetry data along the Northern Vøring transect. It reasonably predicts an emergent outer margin followed by a deep Hel Graben and a shallow Trøndelag Platform at the base Eocene.

The late Paleocene-Eocene mantle thinning alone contributes to a modest outer margin uplift through thermal expansion of mantle rocks (model Plume gives a ca. 700 m deep outer margin, that is 200-m shallower than for the ca. 900-m deep outer margin for the reference model Ref, compare black and red lines on Figure 8b).

The addition of magmatic processes in the model PlumeMelt provides an additional ca. 100 m uplift to the outer margin (dashed red line on Figure 8b). Retention of melt below the lithosphere contributes to a locally lighter asthenosphere. The 3-km-thick magmatic underplate emplaced below the crust is lighter than peridotite (3100 kg/m³ vs. 3300 kg/m³). However, it does not significantly contribute to vertical motions because the magmatic underplate also locally replaces lighter crust.

At last, mantle phase transitions significantly contribute to the outer margin uplift at base Eocene. The additional contribution is ca. 400 m compared to model PlumeMelt (compare dashed and dotted red lines in Figure 8b). During the late Paleocene-Eocene mantle thinning, the upper lithosphere rapidly warms, for example, temperature increases from 700 to 1100°C at 55-km depth, whereas pressure hardly changes. This causes phase transition from dense garnet (3330 kg/m³) to light garnet (3280 kg/m³). The garnet-spinel phase transition in the deeper mantle provides enough density reduction (ca. 50 kg/m³ over a ca. 50 km deep mantle column) to cause temporary uplift and emergence of the outer margin.

6.5 | Possible causes for the two thermal scenarios

We have considered the two thermal scenarios whereby mantle thinning is imposed either *during* the last rifting event or *at the breakup time* in order to approximate mantle

dynamics processes. Possible mantle processes include SSC during the last rifting event and the emplacement of a mantle plume in the Eocene.

The late-Cretaceous-Paleocene rifting event creates lateral variations in thermal structure and density from rift centre to flanks that may drive SSC cells. The pronounced mantle thinning imposed during this last rifting event can then be interpreted as the addition of (1) the increased strong return upward motion of mantle beneath the rift as would be expected by SSC (Duvernay et al., 2021; Huisman et al., 2001) added to (2) the pure shear stretching and upwelling of the mantle asthenosphere occurring because of lithosphere extension (McKenzie, 1978). The downwelling mantle below rift flanks cannot be approximated though. But the approximation remains valid because downwelling limbs are expected to occur far from the upwelling mantle, a few 100 km away according to numerical experiments (van Wijk et al., 2008).

The mantle thinning imposed during the last late Cretaceous-Paleocene rifting event can alternatively be understood as the emplacement of a mantle plume beneath the Vøring Margin. However, the timing does not fit the thermal anomaly emplacement in the area interpreted to be late Paleocene to early Eocene (Skogseid et al., 2000).

On the contrary, the timing of the second thermal scenario (with late Paleocene-early Eocene mantle thinning during the breakup time) fits well with the emplacement of the Iceland plume in the NE Atlantic area. However, interpreting the late Paleocene-early Eocene mantle thinning as SSC is more difficult because thermal cooling has reduced the lateral gradient in temperature and density between the Last-Cretaceous—Paleocene rift centre and flanks.

6.6 | Nature of LCBs

6.6.1 | Nature of the LCB in the outer margin

Unravelling the nature of the outer LCB is crucial to understand the deep structure and tectonic evolution of the volcanic margins and its implications in terms of crustal thinning, heat flow and vertical motion. A model involving a mixture of rocks with contrasting physical properties is in agreement with the large variation in V_p (7.1–7.8 km/s) and relatively low V_p/V_s ratios (1.7–1.85) documented within the LCB by Mjelde et al. (2002). Furthermore, geochemical analyses of sill intrusion on the Vøring Margin demonstrate that the LCB can be explained as a heterogeneous mixture of cumulates associated with the opening related magmatism, and less dense rocks such as the old continental basement (Neumann et al., 2013).

Wangen et al. (2011) also concluded that a scenario involving a LCB constituted solely of underplated material would require an unrealistic amount of pre-breakup extension. A scenario where underplating or lower crustal intrusion (magmatic addition) accounts for the maximum half of the LCB is more likely. The LCB likely represents a complex mixture of pre- to syn-breakup mafic and ultramafic rocks (cumulates and sills) and old metamorphic rocks such as granulites and eclogites (Abdelmalak et al., 2017; Ebbing et al., 2006; Gernigon et al., 2003, 2004, 2006). An increasing degree of melting toward the breakup axis is responsible for an increasing proportion of cumulates and sill intrusions in the lower crust.

The non-melting model Plume predicts a ca. 20-km-deep Moho below the outer margin. This is shallower than the ca. 25-km-deep observed Moho for the LCB with 0% magmatic addition (Figure 10a). Melting model PlumeMelt (shown in Figure 10b), gives a Moho that is less than 20-km-deep below the outer margin. This depth is close to the depth of the Moho for LCB with a 100%

magmatic addition (Figure 10b). This model predicts the magmatic underplate extends and tapers below Nyk High, 50 km west of the Utgard High. This is a bit shorter than suggested by the sill distribution.

6.6.2 | Nature of the LCB below the central margin

Several authors suggest the nature of LCBs below hyper-extended basins in the central and inner margin is different from the outer LCBs (e.g. Lundin & Doré, 2011). Reynisson et al. (2010) suggest the outer LCBs are magmatic but the central LCB is rather made of serpentinized mantle. According to our melting models SSCMelt, PlumeMelt and PlumeMeltPT0, it is very difficult to produce magmatic LCBs east of the Hel Graben, below the central margin, because it is located too far from the source of melting. However, in the serpentinized model, RefSerp33 conditions are reunited to create patches of

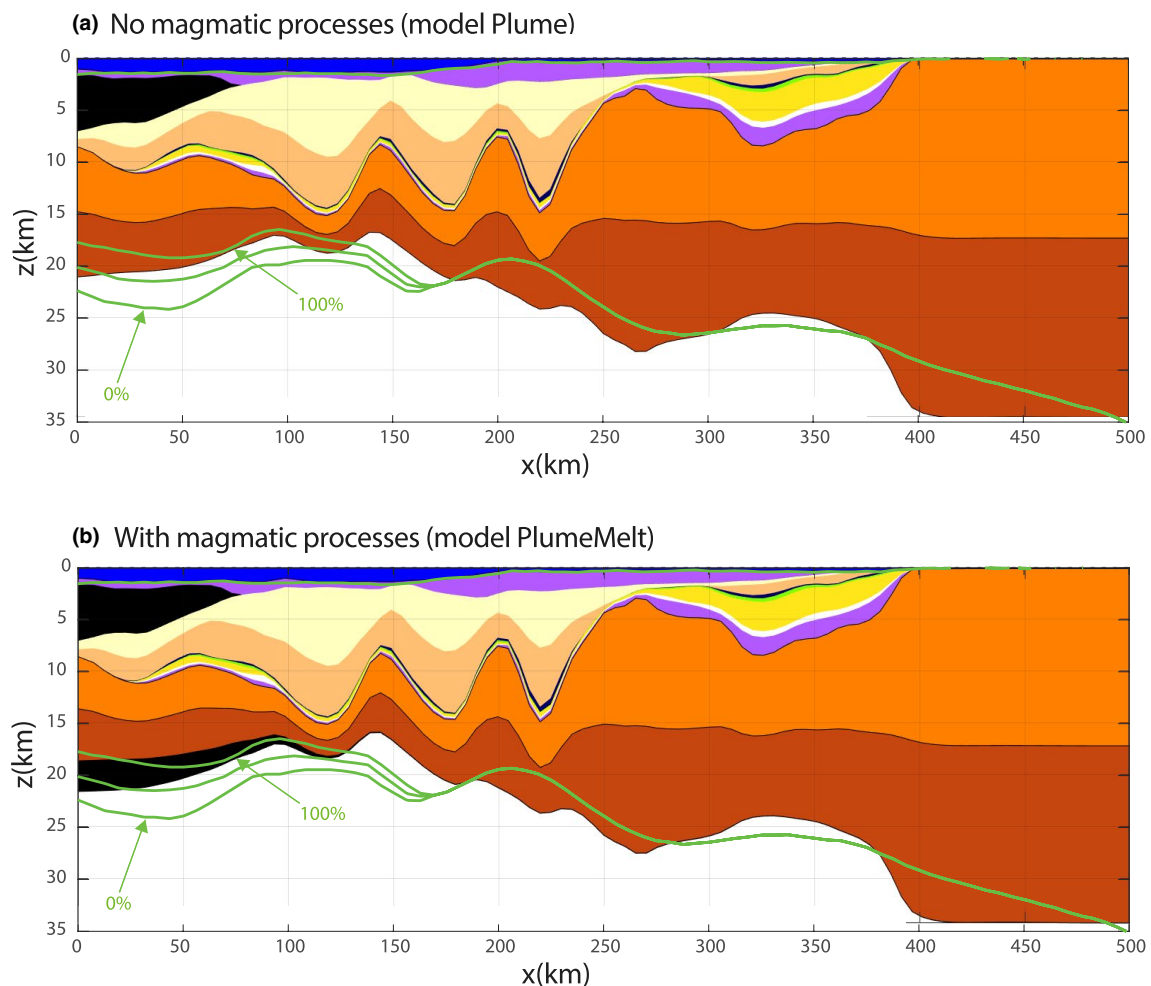
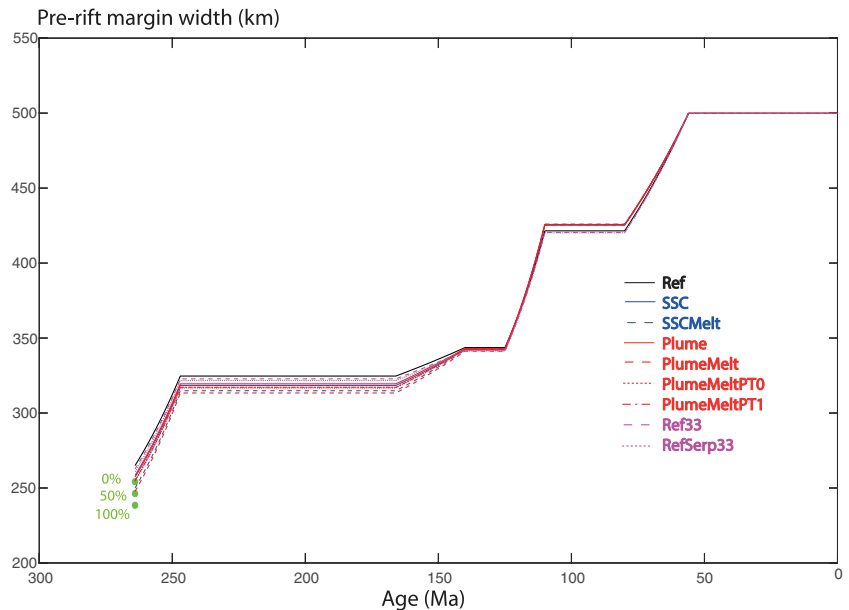


FIGURE 10 Present-day model cross-sections for (a) for the magmatic model M2 and (b) for the magmatic model PlumeMelt. The green line represents the observed crustal Moho for LCB with different magmatic additions (0%, 50% and 100%)

FIGURE 11 Modelled pre-drift margin widths through time for the different models. The green dots represent the pre-drift margin widths estimated from the observed stretching factors for different interpretations of the LCB (0%, 50% and 100% magmatic LCB)



the partially serpentinized mantle below the Hel Graben and Nyk High considering an initial crust is thin enough (33 km) (Figure 9). Unfortunately, the paleo water depth predicted by this model (dotted magenta line on Figure 8b) shows an important misfit compared to the interpreted paleobathymetry. Moreover, the distribution of sills in the Vøring Basin suggests that magmatism; hence, magmatic addition to the LCB, extends east to the Utgard high (Abdelmalak et al., 2017). This argues against a serpentinized mantle below the central part of the margin.

6.7 | Paleogeometry of the Vøring Margin since the late Paleozoic

Available deep seismic data allow to estimate the crustal stretching factor, hence, the total extension the margin has experienced since the beginning of rifting in the late Paleozoic. The width of the margin before the extension is estimated from the stretching factor. Depending on the interpretation of the LCB, the initial width is 254 km (for a 0% magmatic underplate), 246 km (for a 50% magmatic underplate) and 238 km (for a 100% magmatic underplate). However, this method does not allow to quantify the amount of extension caused by each individual rift event. It is, therefore, difficult to reconstruct the geometry of the margin at different steps of its evolution since the late Paleozoic.

Fortunately, the forward thermal-kinematic modelling of the Vøring Margin provides the crustal stretching factors, and the corresponding amount of extension, for each rifting phase making it possible to reconstruct the geometrical evolution of the margin. For each model, the transect length before each rifting event is computed from

the distribution of stretching factors (Figure 11). The predicted pre-rift width does not differ a lot between each model. The present-day length of the profile is 500 km, whereas the initial length varies from 241 to 265 km depending on the model, close to the values estimated from the seismic data. The standard model gives the widest initial margin (265 km). In addition, each model shows similar evolution meaning it gives a similar amount of widening at each rifting phase. The mid-Cretaceous rifting event yields the largest widening (80 km) for all the models. Based on the estimates of the transect length for the Northern Vøring transect through the Vøring margin history, the geometry of the margin since the late Paleozoic can be reconstructed.

7 | CONCLUSION

We have computed 2D models of basin evolution based on an inverse-scheme approach to simulate the thermal and tectonic history of the multirift Vøring margin along a seismic transect crossing its northern part. Two tectono-magmatic scenarios are evaluated: (1) The first scenario including pronounced mantle thinning during the last rifting event leading to breakup and that can be understood as sub-lithospheric active processes, such as SSC and (2) a second scenario including thermal thinning at the time of breakup after the last rifting event and that can be interpreted as the emplacement of the late Paleocene-early Eocene plume beneath the outer margin. The following conclusions are drawn:

1. The standard model of extension satisfactorily reproduces the observed stratigraphy of the inner margin

assuming four rifting phases (late Permian, late Jurassic-early Cretaceous, mid-Cretaceous and late Cretaceous-Paleocene). However, it fails to reproduce key observations at the outer margin.

- Models incorporating late Paleocene-early Eocene mantle thinning taking into account magmatic processes (melt retention and magmatic underplate) and mantle phase transitions can satisfactorily reproduce the anomalies (high vitrinite reflectance values, magmatic LCB and base Eocene uplift) of the outer margin. The late Paleocene-early Eocene mantle thinning scenario can be interpreted as the emplacement of the Iceland mantle plume. It is less likely to be SSC.
- If the initial crust is thin enough, crustal-scale brittle faulting can occur allowing for water to penetrate the upper mantle below the highly-extended Vøring Basin triggering partially serpentinization of the mantle with seismic and gravity signals similar to inner LCBs.
- Our modelling exercise predicts similar pre-rift margin width whatever the models. The initial pre-rift margin width varies between 241 and 265 km depending on the models for a final width of 500 km. The major phases of widening are late Permian and mid-Cretaceous.

ACKNOWLEDGEMENTS

The present work is part of the CEED Mod project funded by Vår Energi, Lundin Norway and Aker BP and ARCEX (Research Centre for Arctic Petroleum Exploration), which is funded by the Research Council of Norway and # industry partners. We also recognize the Research Council of Norway through its Centres of Excellence funding scheme, Project Number 223272. We thank the reviewers Laurent Gernigon, John Armitage and Jolante van Wijk, the editor, and associated editor Craig Magee for their helpful comments and guidance that improved the paper.

CONFLICT OF INTEREST

There is no conflict of interest to declare.

PEER REVIEW

The peer review history for this article is available at <https://publons.com/publon/10.1111/bre.12637>.

DATA AVAILABILITY STATEMENT

The data that support the findings of this study are available from the corresponding author upon reasonable request.

ORCID

Sébastien Gac  <https://orcid.org/0000-0002-6318-5116>
 Mansour M. Abdelmalak  <https://orcid.org/0000-0003-2200-1074>

Jan Inge Faleide  <https://orcid.org/0000-0001-8032-2015>

[org/0000-0001-8032-2015](https://orcid.org/0000-0001-8032-2015)

Daniel W. Schmid  <https://orcid.org/0000-0002-4271-0858>

[org/0000-0002-4271-0858](https://orcid.org/0000-0002-4271-0858)

Dmitry Zastrozhnov  <https://orcid.org/0000-0003-2354-4708>

[org/0000-0003-2354-4708](https://orcid.org/0000-0003-2354-4708)

REFERENCES

- Abdelmalak, M. M., Faleide, J. I., Planke, S., Gernigon, L., Zastrozhnov, D., Shephard, G. E., & Myklebust, R. (2017). The T-reflection and the deep crustal structure of the Vøring Margin offshore mid-Norway. *Tectonics*, *36*, 2497–2523. <https://doi.org/10.1002/2017TC004617>
- Abdelmalak, M. M., Planke, S., Faleide, J. I., Jerram, D. A., Zastrozhnov, D., Eide, S., & Myklebust, R. (2016). The development of volcanic sequences at rifted margins: New insights from the structure and morphology of the Vøring Escarpment, mid-Norwegian Margin. *Journal of Geophysical Research: Solid Earth*, *121*, 5212–5236. <https://doi.org/10.1002/2015JB012788>
- Berndt, C., Planke, S., Alvestad, E., Tsikalas, F., & Rasmussen, T. (2001). Seismic volcanostratigraphy of the Norwegian margin: Constraints on tectonomagmatic break-up processes. *Journal of the Geological Society*, *158*, 413–426. <https://doi.org/10.1144/jgs.158.3.413>
- Blystad, P., Brekke, H., Færseth, R. B., Larsen, B. T., Skogseid, J., & Tørudbakken, B. (1995). Structural elements of the Norwegian continental shelf. Part II: The Norwegian Sea Region. *Norwegian Petroleum Directorate Bulletin*, *8*, 45.
- Boutillier, R. R., & Keen, C. E. (1999). Small-scale convection and divergent plate boundaries. *Journal of Geophysical Research*, *10*, 7389–7403. <https://doi.org/10.1029/1998JB900076>
- Braun, J., & Beaumont, C. (1989). A physical explanation of the relation between flank uplifts and the breakup unconformity at rifted continental margins. *Geology*, *17*, 760–764. [https://doi.org/10.1130/0091-7613\(1989\)017<0760:APEOTR>2.3.CO;2](https://doi.org/10.1130/0091-7613(1989)017<0760:APEOTR>2.3.CO;2)
- Breivik, A. J., Faleide, J. I., Mjelde, R., & Flueh, E. (2009). Magma productivity and early seafloor spreading rate correlation on the northern Vøring Margin, Norway—Constraints on mantle melting. *Tectonophysics*, *468*, 206–223. <https://doi.org/10.1016/j.tecto.2008.09.020>
- Breivik, A. J., Mjelde, R., Raum, T., Faleide, J. I., Murai, Y., & Flueh, E. R. (2010). Crustal structure beneath the Trøndelag Platform and adjacent areas of the mid-Norwegian margin, as derived from wide-angle seismic and potential field data. *Norwegian Journal of Geology*, *90*, 141–161.
- Brekke, H. (2000). The tectonic evolution of the Norwegian Sea continental margin with emphasis on the Vøring and More Basins. In A. Nottvedt, S. Olaussen, B. Torudbakken, R. H. Gabrielsen, H. Brekke, O. Birkeland, & J. Skogseid (Eds.), *Dynamics of the Norwegian Margin* (Vol. 167, pp. 327–378). Geol. Soc. Spec. Publ.
- Buck, W. R. (1986). Small-scale convection induced by passive rifting: The cause of uplift of rift shoulders. *Earth and Planetary Science Letters*, *77*, 362–372.
- Clark, S. A., Glørstad-Clark, E., Faleide, J. I., Schmid, D., Hartz, E. H., & Fjeldskaar, W. (2014). Southwest Barents Sea rift basin evolution: Comparing results from backstripping and

- time-forward modelling. *Basin Research*, 26, 550–566. <https://doi.org/10.1111/bre.12039>
- Cunha, T. A., Rasmussen, H., Villinger, H., & Akinwumiju, A. A. (2021). Burial and heat flux modelling along a Southern Vøring Basin transect: Implications for the petroleum systems and thermal regimes in the deep mid-Norwegian sea. *Geosciences*, 11, 1–27. <https://doi.org/10.3390/geosciences11050190>
- Duvernay, T., Davies, D. R., Mathews, C. R., Gibson, A. H., & Kramer, S. C. (2021). Linking intraplate volcanism to lithospheric structures and asthenospheric flow. *Geochemistry, Geophysics, Geosystems*, 22, e2021GC009953.
- Ebbing, J., Lundin, E., Olesen, O., & Hamsen, E. K. (2006). The mid-Norwegian margin: A discussion of crustal lineaments, mafic intrusions, and remnants of the Caledonian root by 3D density modelling and structural interpretation. *Journal of the Geological Society*, 163, 47–59.
- Eldholm, O., & Grue, K. (1994). North Atlantic volcanic margins: Dimensions and production rates. *Journal of Geophysical Research: Solid Earth*, 99, 2955–2968.
- Faleide, J. I., Tsikalas, F., Breivik, A. J., Mjelde, R., Ritzmann, O., Engen, O., Wilson, J., & Eldholm, O. (2008). Structure and evolution of the continental margin off Norway and Barents Sea. *Episodes*, 3, 82–91.
- Fjeldskaar, W., Grunnaleite, I., Zweigel, J., Mjelde, R., Faldeide, J. I., & Wilson, J. (2009). Modelled palaeo-temperature on Voring, offshore Mid-Norway—The effect of the lower crustal body. *Tectonophysics*, 474, 544–558.
- Fjeldskaar, W., Helset, H. M., Johansen, H., Grunnaleiten, I., & Horstad, I. (2008). Thermal modelling of magmatic intrusions in the Gjallar Ridge, Norwegian Sea: Implications for Vitrinite reflectance and hydrocarbon maturation. *Basin Research*, 20, 143–159. <https://doi.org/10.1111/j.1365-2117.2007.00347.x>
- Fjeldskaar, W., TerVoorde, M., Johansen, H., Christiansson, P., Faleide, J. I., & Cloetingh, S. A. P. L. (2004). Numerical simulation of rifting in the northern Viking Graben: The mutual effect of modeling parameters. *Tectonophysics*, 382, 189–212.
- Funck, T., Geissler, W. H., Kimbell, G. S., Gradmann, S., Erlendsson, Ö., McDermott, K., & Petersen, U. K. (2017). Moho and basement depth in the NE Atlantic Ocean based on seismic refraction data and receiver functions. In G. Péron-Pinvidic, J. R. Hopper, M. S. Stoker, C. Gaina, J. C. Doornenbal, T. Funck, & U. Årting (Eds.), *The NE Atlantic Region: A reappraisal of crustal structure, tectonostratigraphy and magmatic evolution* (Vol. 447, pp. 207–231). Geological Society, London, Special Publications.
- Gac, S., Hansford, P. A., & Faleide, J. I. (2018). Basin modelling of the SW Barents Sea. *Marine and Petroleum Geology*, 95, 167–187. <https://doi.org/10.1016/j.marpetgeo.2018.04.022>
- Gernigon, L., Franke, D., Geoffroy, L., Schiffer, C., Foulger, G. R., & Stoker, M. (2020). Crustal fragmentation, magmatism, and the diachronous opening of the Norwegian-Greenland Sea. *Earth Science Reviews*, 206, 102839. <https://doi.org/10.1016/j.earscirev.2019.04.011>
- Gernigon, L., Lucazeau, F., Brigaud, F., Ringenbach, J.-C., Planke, S., & Le Gall, B. (2006). A moderate melting model for the Vøring margin (Norway) based on structural observations and a thermo-kinematical modelling: Implication for the meaning of the lower crustal bodies. *Tectonophysics*, 412(3), 255–278. <https://doi.org/10.1016/j.tecto.2005.10.038>
- Gernigon, L., Ringenbach, J.-C., Planke, S., & Le Gall, B. (2004). Deep structures and breakup along volcanic rifted margins: Insights from integrated studies along the outer Vøring Basin (Norway). *Marine and Petroleum Geology*, 21(3), 363–372. <https://doi.org/10.1016/j.marpetgeo.2004.01.005>
- Gernigon, L., Ringenbach, J. C., Planke, S., Le Gall, B., & Jonquet-Kolsto, H. (2003). Extension, crustal structure and magmatism at the outer Vøring Basin, Norwegian margin. *Journal of the Geological Society*, 160, 197–208.
- Gradstein, F. M., Anthonissen, E., Brunstad, H., Charnock, M., Hammer, Ø., Hellem, T., & Lervik, K. S. (2010). Norwegian offshore stratigraphic lexicon (NORLEX). *Newsletters on Stratigraphy*, 44, 73–86. <https://doi.org/10.1127/0078-0421/2010/0005>
- Griffiths, R. W., & Campbell, I. H. (1990). Stirring and structure in mantle starting plumes. *Earth and Planetary Science Letters*, 99, 66–78. [https://doi.org/10.1016/0012-821X\(90\)90071-5](https://doi.org/10.1016/0012-821X(90)90071-5)
- Hartz, E. B., Medvedev, S., & Schmid, D. W. (2016). Development of sedimentary basins: Differential stretching, phase transitions, shear heating and tectonic pressure. *Basin Research*, 29, 591–604. <https://doi.org/10.1111/bre.12189>
- Holbrook, W. S., Larsen, H. C., Korenaga, J., Dahl-Jensen, T., Reid, I. D., Kelemen, P. B., Hopper, J. R., Kent, G. M., Lizarralde, D., Bernstein, S., & Detrick, R. S. (2001). Mantle thermal structure and active upwelling during continental breakup in the North Atlantic. *Earth and Planetary Science Letters*, 190, 251–266. [https://doi.org/10.1016/S0012-821X\(01\)00392-2](https://doi.org/10.1016/S0012-821X(01)00392-2)
- Huismans, R. S., Podladchikov, Y. Y., & Cloetingh, S. A. P. L. (2001). Transition from passive to active rifting: Relative importance of asthenospheric doming and passive extension of the lithosphere. *Journal of Geophysical Research*, 106, 11271–11291. <https://doi.org/10.1029/2000JB900424>
- Jarvis, G. T., & McKenzie, D. P. (1980). Sedimentary basin formation with finite extension rates. *Earth and Planetary Science Letters*, 48, 42–52. [https://doi.org/10.1016/0012-821X\(80\)90168-5](https://doi.org/10.1016/0012-821X(80)90168-5)
- Jaupart, C., Sclater, J., & Simmons, G. (1981). Heat flow studies: Constraints on the distribution of uranium, thorium and potassium in the continental crust. *Earth and Planetary Science Letters*, 52, 328–344. [https://doi.org/10.1016/0012-821X\(81\)90187-4](https://doi.org/10.1016/0012-821X(81)90187-4)
- Kaus, B. J. P., Connolly, J. A. D., Podladchikov, Y. Y., & Schmalholz, S. (2005). Effect of mineral phase transitions on sedimentary basin subsidence and uplift. *Earth and Planetary Science Letters*, 233, 213–228. <https://doi.org/10.1016/j.epsl.2005.01.032>
- Kelemen, P. B., & Holbrook, W. S. (1995). Origin of thick, high-velocity igneous crust along the U.S. East Coast Margin. *Journal of Geophysical Research: Solid Earth*, 100, 10077–10094. <https://doi.org/10.1029/95JB00924>
- Kjennerud, T., & Vergara, L. (2005). Cretaceous to Palaeogene 3D palaeobathymetry and sedimentation in the Vøring Basin, Norwegian Sea. In A. G. Doré & B. A. Vining (Eds.), *Petroleum geology: North-West Europe and global perspectives—Proceedings of the 6th Petroleum Geology Conference* (pp. 815–831). Petroleum Geology Conferences Ltd. Geological Society.
- Lawver, L. A., & Müller, R. D. (1994). Iceland hot spot track. *Geology*, 22, 311–314. [https://doi.org/10.1130/0091-7613\(1994\)022<0311:IHT>2.3.CO;2](https://doi.org/10.1130/0091-7613(1994)022<0311:IHT>2.3.CO;2)
- Lundin, E., & Doré, A. (1997). A tectonic model for the Norwegian passive margin with implications for the NE Atlantic: Early Cretaceous to break-up. *Journal of the Geological Society*, 154, 545–550. <https://doi.org/10.1144/gsjgs.154.3.0545>
- Lundin, E. R., & Doré, A. G. (2011). Hyperextension, serpentinization, and weakening: A new paradigm for rifted margin

- compressional deformation. *Geology*, 39, 347–350. <https://doi.org/10.1130/G31499.1>
- Maystrenko, Y. P., & Gernigon, L. (2018). 3-D temperature distribution beneath the Mid-Norwegian continental margin (the Vøring and Møre basins). *Geophysical Journal International*, 212, 694–724.
- McKenzie, D. (1978). Some remarks on development of sedimentary basins. *Earth and Planetary Science Letters*, 40, 25–32.
- Meyer, R., Hertogen, J., Pedersen, R. B., Viereck-Gotte, L., & Abratis, M. (2007). Crustal-mantle melt interactions during continental breakup at the early Paleocene Vøring Plateau, North Atlantic igneous province. *Geochimica et Cosmochimica Acta*, 71(15), A661.
- Mjelde, R., Digranes, P., Shimamura, H., Shiobara, H., Kodaira, S., Brekke, H., Egebjerg, T., Sørensen, N., & Thorbjørnsen, S. (1998). Crustal structure of the northern part of the Vøring Basin, mid-Norway margin, from wide-angle seismic and gravity data. *Tectonophysics*, 293, 175–205.
- Mjelde, R., Kasahara, J., Shimamura, H., Kamimura, A., Kanazawa, T., Kodaira, S., Raum, T., & Shiobara, H. (2002). Lower crustal seismic velocity-anomalies; magmatic underplating or serpentinized peridotite? Evidence from the Vøring Margin, NE Atlantic. *Marine Geophysical Researches*, 23(2), 169–183.
- Mutter, J. C., Buck, W. R., & Zehnder, C. M. (1988). Convective partial melting, 1. A model for the formation of thick basaltic sequences during the initiation of spreading. *Journal of Geophysical Research*, 93, 1031–1048. <https://doi.org/10.1029/JB093iB02p01031>
- Neumann, E.-R., Svensen, H., Tegner, C., Planke, S., Thirlwall, M., & Jarvis, K. E. (2013). Sill and lava geochemistry of the mid-Norway and NE Greenland conjugate margins. *Geochemistry, Geophysics, Geosystems*, 14, 3666–3690. <https://doi.org/10.1002/ggge.20224>
- Njone, I. (2014). *Hydrothermal vent activities at the Gjallar Ridge in the Vøring Basin, mid-Norway* [Master's thesis]. The Arctic University of Norway.
- Petersen, K. D., Schiffer, C., & Nagel, T. (2018). LIP formation and protracted lower mantle upwelling induced by rifting and delamination. *Scientific Reports*, 8, 1–11. <https://doi.org/10.1038/s41598-018-34194-0>
- Petrini, K. A. T. E., Connolly, J. A. D., & Podladchikov, Y. Y. (2001). A coupled petrological-tectonic model for sedimentary basin evolution: The influence of metamorphic reactions on basin subsidence. *Terra Nova*, 13, 354–359. <https://doi.org/10.1046/j.1365-3121.2001.00371.x>
- Planke, S., Rasmussen, T., Rey, S. S., & Myklebust, R. (2005). Seismic characteristics and distribution of volcanic intrusions and hydrothermal vent complexes in the Vøring and Møre basins. In A. G. Dore & B. A. Vining (Eds.), *Petroleum geology: North-West Europe and global perspectives—Proceedings of the 6th Petroleum Geology Conference* (pp. 833–844). Geological Society.
- Podladchikov, Y. Y., Poliakov, A. N. B., & Yuen, D. A. (1994). The effect of lithospheric phase transitions on subsidence of extending continental lithosphere. *Earth and Planetary Science Letters*, 124, 95–103. [https://doi.org/10.1016/0012-821X\(94\)00074-3](https://doi.org/10.1016/0012-821X(94)00074-3)
- Quirk, D. G., & Rüpke, L. H. (2018). Melt-induced buoyancy may explain the elevated rift-rapid sag paradox during breakup of continental plates. *Scientific Reports*, 8, 9985. <https://doi.org/10.1038/s41598-018-27981-2>
- Ranalli, G., & Murphy, D. C. (1987). Rheological stratification of the lithosphere. *Tectonophysics*, 132(4), 281–295. [https://doi.org/10.1016/0040-1951\(87\)90348-9](https://doi.org/10.1016/0040-1951(87)90348-9)
- Ren, S. C., Faleide, J. I., Eldholm, O., Skogseid, J., & Gradstein, F. (2003). Late Cretaceous-Paleocene tectonic development of the NW Vøring Basin. *Marine and Petroleum Geology*, 20, 177–206. [https://doi.org/10.1016/S0264-8172\(03\)00005-9](https://doi.org/10.1016/S0264-8172(03)00005-9)
- Reynisson, R. F., Ebbing, J., Lundin, E., & Osmundsen, P. T. (2010). Properties and distribution of lower crustal bodies on the mid-Norwegian margin. *Geological Society, London, Petroleum Geology Conference Series*, 7, 843–854. <https://doi.org/10.1144/0070843>
- Roberts, A. M., Corfield, R. I., Kuszniir, N. J., Matthews, S. J., Hansen, E.-K., & Hooper, R. J. (2009). Mapping palaeostructure and palaeobathymetry along the Norwegian Atlantic continental margin, Møre and Voring basins. *Petroleum Geoscience*, 15, 27–43. <https://doi.org/10.1144/1354-079309-804>
- Royden, L., & Keen, C. E. (1980). Rifting process and thermal evolution of the continental margin of eastern Canada determined from subsidence curves. *Earth and Planetary Science Letters*, 51, 343–361. [https://doi.org/10.1016/0012-821X\(80\)90216-2](https://doi.org/10.1016/0012-821X(80)90216-2)
- Rüpke, L. H., Schmalholz, S. M., Schmid, D. W., & Podladchikov, Y. Y. (2008). Automated thermotectonostratigraphic basin reconstruction: Viking Graben case study. *AAPG Bulletin*, 92(3), 309–326. <https://doi.org/10.1306/11140707009>
- Rüpke, L. H., Schmid, D. W., Hartz, E. W., & Martinsen, B. (2010). Basin modelling of a transform margin setting: Structural, thermal and hydrocarbon evolution of the Tano Basin Ghana. *Petroleum Geoscience*, 16(3), 283–298. <https://doi.org/10.1144/1354-079309-905>
- Rüpke, L. H., Schmid, D. W., Perez-Gussinye, M., & Hartz, E. (2013). Interrelation between rifting, faulting, sedimentation, and mantle serpentinization during continental margin formation-including examples from the Norwegian Sea. *Geochemistry, Geophysics, Geosystems*, 14, 4351–4369. <https://doi.org/10.1002/ggge.20268>
- Sclater, J. G., & Christie, P. A. F. (1980). Continental stretching: An explanation of the post-mid-Cretaceous subsidence of the central North Sea basin. *Journal of Geophysical Research*, 85, 3711–3739.
- Simon, K., Huismans, R. S., & Beaumont, C. (2009). Dynamical modelling of lithospheric extension and small-scale convection: Implications for magmatism during the formation of volcanic rifted margins. *Geophysical Journal International*, 176(1), 327–350. <https://doi.org/10.1111/j.1365-246X.2008.03891.x>
- Simon, N. S. C., & Podladchikov, Y. Y. (2008). The effect of mantle composition on density in the extending lithosphere. *Earth and Planetary Science Letters*, 272, 148–157. <https://doi.org/10.1016/j.epsl.2008.04.027>
- Skelton, A., Whitmarsh, R., Arghe, F., Crill, P., & Koyi, H. (2005). Constraining the rate and extent of mantle serpentinization from seismic and petrological data: Implications for chemosynthesis and tectonic processes. *Geofluids*, 5(3), 153–164. <https://doi.org/10.1111/j.1468-8123.2005.00111.x>
- Skogseid, J., Planke, S., Faleide, J. I., Pedersen, T., Eldholm, O., & Neverdal, F. (2000). NE Atlantic continental rifting and volcanic margin formation. In A. Nottvedt, B. T. Larsen, R. H. Gabrielsen, S. Olaussen, B. Torudbakken, J. Skogseid, H. Brekke, & O. Birkeland (Eds.), *Dynamics of the Norwegian Margin* (Vol. 167, pp. 295–326). Geol. Soc. Spec. Publ.

- Theissen, S., & Rüpke, L. H. (2009). Feedbacks of sedimentation on crustal heat flow: New insights from the Vøring Basin, Norwegian Sea. *Basin Research*, 22, 976–990. <https://doi.org/10.1111/j.1365-2117.2009.00437.x>
- Theissen-Krah, S., Zastrozhnov, D., Abdelmalak, M., Schmid, D., Faleide, J. I., & Gernigon, L. (2017). Tectonic evolution and extension at the Møre Margin-Offshore mid-Norway. *Tectonophysics*, 721, 227–238. <https://doi.org/10.1016/j.tecto.2017.09.009>
- Tsikalas, F., Faleide, J. I., Eldholm, O., & Blaich, O. A. (2012). The NE Atlantic conjugate margins. In D. G. Roberts & A. W. Bally (Eds.), *Regional geology and tectonics: Phanerozoic passive margins, cratonic basins and global tectonic maps* (pp. 141–200). Elsevier.
- Turcotte, D. L., & Schubert, G. (2002). *Geodynamics* (2nd ed., p. 456). Cambridge University Press.
- van Wijk, J. W., Huismans, R. S., Ter Voorde, M., & Cloetingh, S. A. P. L. (2001). Melt generation at volcanic continental margins: No need for a mantle plume? *Geophysical Research Letters*, 28(20), 3995–3998. <https://doi.org/10.1029/2000GL012848>
- van Wijk, J., van Hunen, J., & Goes, S. (2008). Small-scale convection during continental rifting: Evidence from the Rio Grande rift. *Geology*, 36, 575–578.
- Wangen, M., Mjelde, R., & Faleide, J. I. (2011). The extension of the Vøring margin (NE Atlantic) in case of different degrees of magmatic underplating. *Basin Research*, 23(1), 83–100. <https://doi.org/10.1111/j.1365-2117.2010.00467.x>
- Watts, A. B., Karner, G. D., & Steckler, M. S. (1982). Lithospheric flexure and the evolution of sedimentary basins. *Philosophical Transactions of the Royal Society of London. Series A, Mathematical and Physical Sciences*, 305, 249–281.
- White, R. S., & Smith, L. K. (2009). Crustal structure of the Hatton and the conjugate East Greenland rifted volcanic margins, NE Atlantic. *Journal of Geophysical Research: Solid Earth*, 114, B02305. <https://doi.org/10.1029/2008JB005856>
- White, R. S., Smith, L. K., Roberts, A. W., Christie, P. A. F., Kuszniir, N. J., & The Rest of the iSIMM Team. (2008). Lower-crustal intrusion on the North Atlantic continental margin. *Nature*, 452, 460–465. <https://doi.org/10.1038/nature06687>
- White, R. S., Spence, G. D., Fowler, S. R., McKenzie, D. P., Westbrook, G. K., & Bowen, A. N. (1987). Magmatism at rifted continental margins. *Nature*, 330, 439–444. <https://doi.org/10.1038/330439a0>
- Yamasaki, T., & Nakada, M. (1997). The effects of the spinel–garnet phase transition on the formation of rifted sedimentary basins. *Geophysical Journal International*, 130, 681–692. <https://doi.org/10.1111/j.1365-246X.1997.tb01862.x>
- Zastrozhnov, D., Gernigon, L., Gogin, I., Abdelmalak, M. M., Planke, S., Faleide, J. I., Eide, S., & Myklebust, R. (2018). Cretaceous–paleocene evolution and crustal structure of the northern Vøring margin (offshore mid-Norway): Results from integrated geological and geophysical study. *Tectonics*, 37(2), 497–528.
- Zastrozhnov, D., Gernigon, L., Gogin, I., Planke, S., Abdelmalak, M. M., Polteau, S., Faleide, J. I., Manton, B., & Myklebust, R. (2020). Regional structure and polyphased Cretaceous–Paleocene rift and basin development of the mid-Norwegian volcanic passive margin. *Marine and Petroleum Geology*, 115, 104269. <https://doi.org/10.1016/j.marpetgeo.2020.104269>

How to cite this article: Gac, S., Abdelmalak, M. M., Faleide, J. I., Schmid, D. W., & Zastrozhnov, D. (2021). Basin modelling of a complex rift system: The Northern Vøring Volcanic Margin case example. *Basin Research*, 00, 1–25. <https://doi.org/10.1111/bre.12637>